HELSINGIN YLIOPISTO
HELSINGFORS UNIVERSITET
UNIVERSITY OF HELSINKI

Marine ecosystem changes and their linkages to climate and terrestrial freshwater inputs in a Northeast Greenland fjord over the Holocene

Meri Marianne Mäkelä
University of Helsinki
Faculty of Biological and Environmental Sciences
Master's Programme in Environmental Change and Global Sustainability
Master's Thesis
May 2021

Tiedekunta - Fakultet - Faculty Faculty of Biological and Environmental sciences		
Tekijä - Författare – Author Meri Marianne Mäkelä		
Työn nimi - Arbetets titel –Title Marine ecosystem changes and their linkages to climate and terrestrial freshwater inputs in a Northeast Greenland fjord over the Holocene		
Oppiaine - Läroämne - Subject Master's programme in Environmental Change and Global Sustainability		
Työn laji/ Ohjaaja - Arbetets art/Handledare - Level/Instructor Master's Thesis/ Maija Heikkilä and Kaarina Weckström	Aika - Datum - Month and year May 2021	Sivumäärä - Sidoantal - Number of pages 60 pages

Tiivistelmä - Referat – Abstract

The present retreat of the Greenland Ice Sheet will increase the amount of fjords surrounded only by land-terminating glaciers in the future. As in the Arctic, productivity is generally lower at these kinds of fjord systems than in the ones surrounded by marine-terminating glaciers, this will most likely affect the productivity and ecosystem structure of coastal marine areas. Paleorecords of past coastal ecosystems can improve our understanding of the drivers of Arctic coastal ecosystem change and provide possible future scenarios. At present, there are not many high-resolution marine ecosystem reconstructions from the Arctic near-shore areas, and in particular those, which take into account land-derived inputs are lacking.

To provide a detailed reconstruction of coastal marine ecosystem change over the Holocene and study its linkages to climate and terrestrial freshwater inputs, organic-walled palynomorphs (including e.g. dinoflagellate cysts and pollen) and some basic geochemistry (including e.g. total organic carbon, C:N ratio, biogenic silica and stable isotopes of carbon and nitrogen) were examined from two radiometrically dated sediment cores from Young Sound fjord, Northeast Greenland.

The results indicate that the near-shore marine ecosystem in Young Sound is clearly influenced by local forcings, such as terrestrial freshwater and organic matter inputs, during the Holocene. The results also illustrate that these terrestrial inputs affect the ecosystem structure and at least some dimension of ecosystem productivity. This study demonstrates that increasing number of fjords with only land-terminating glaciers in the future will affect marine productivity and ecosystem structure in Greenland's fjord systems, with potential impacts on biodiversity and important fisheries. Studying past ecosystem changes in different fjord systems, and complementing marine records with proxies for terrestrial inputs, would further help constrain the future scenarios along the Greenland shore.

Avainsanat – Nyckelord – Keywords

Paleoecology, the Holocene, dinocysts, Palynomorphs, C:N, $\delta^{13}C$, $\delta^{15}N$, Biogenic silica, total organic carbon, the Arctic, Northeast Greenland, coastal regions, sea-ice, terrestrial inputs

Säilytyspaikka - Förvaringsställe - Where deposited

HELDA - Digital Repository of the University of Helsinki

Muita tietoja - Övriga uppgifter - Additional information

Tiedekunta - Fakultet - Faculty Bio-ja ympäristötieteellinen tiedekunta		
Tekijä - Författare – Author Meri Marianne Mäkelä		
Työn nimi - Arbetets titel –Title Meriekosysteemin Holoseenin aikaiset muutokset Koillis-Grönlannin vuonosysteemissä ja muutosten yhteydet ilmastovaihteluun sekä maalta tulevaan makeaan veteen		
Oppiaine - Läroämne - Subject Ympäristönmuutoksen ja globaalin kestävyyden maisteriohjelma		
Työn laji/ Ohjaaja - Arbetets art/Handledare - Level/Instructor Pro gradu-tutkielma / Maija Heikkilä ja Kaarina Weckström	Aika - Datum - Month and year Toukokuu 2021	Sivumäärä - Sidoantal - Number of pages 60 s.

Tiivistelmä - Referat – Abstract

Grönlannin mannerjään sulaminen lisää tulevaisuudessa sellaisten vuonojen määrää, joita ympäröivät ainoastaan maalle päätyvät jäätiköt. Koska arktisella alueella tuottavuus on yleisesti ottaen alhaisempaa tällaisissa vuonoissa, kuin niissä, joita ympäröivät myös mereen päättyvät jäätiköt, mannerjään vetäytyminen tulee todennäköisesti vaikuttamaan tuottavuuteen ja meriekosysteemien rakenteeseen rannikkoseuduilla. Paleotutkimuksen avulla on mahdollista parantaa ymmärrystämme arktisten rannikkoalueiden muutoksien syistä ja ennustaa tulevaisuuden skenaarioita. Korkea-resoluutioisia arktisten merialueiden rekonstruktioita ei kuitenkaan ole paljoa, ja etenkin sellaiset ovat harvinaisia, jotka ottavat huomioon myös maalta peräisin olevat makean veden ja orgaanisen materiaalin virrat.

Tämän tutkimuksen tarkoituksena on rekonstruoida rannikon meriekosysteemin muutoksia Holoseenin aikana, sekä muutosten yhteyttä ilmastoon ja maalta peräisin oleviin makean veden ja orgaanisen aineksen virtoihin. Tutkimuksessa hyödynnettiin muun muassa panssarisiimalevien kystejä sekä siitepölyä ja geokemiallisia muuttujia (kuten orgaanisen hiilen kokonaismäärää, hiili-typpi suhdetta, biogeenista piitä sekä hiilen ja typen stabiileja isotooppeja) kahdesta radiometrisesti ajoitetusta sedimenttikoorista Young Soundin vuonosysteemistä Koillis-Grönlannista.

Tutkimuksen tulokset osoittavat, että paikalliset tekijät, kuten maalta peräisin olevat makean veden ja orgaanisen aineksen virrat, vaikuttavat rannikon läheiseen meriekosysteemiin Young Soundin vuonossa. Tulosten mukaan nämä mantereelta peräisin olevat virrat vaikuttavat ekosysteemin rakenteeseen ja jossain määrin myös tuottavuuteen. Tutkimuksen perusteella sellaisten vuonojen määrän lisääntyminen, joita ympäröivät pelkästään maalle päättyvät jäätiköt, voi vaikuttaa Grönlannin rannikon vuonosysteemien tuottavuuteen ja ekosysteemien rakenteeseen, ja sitä kautta mahdollisesti myös biodiversiteettiin ja tärkeisiin kalakantoihin. Menneiden ekosysteemien muutosten tutkiminen erilaisissa vuonosysteemeissä, ja merellisten vastemuuttujien täydentäminen myös sellaisilla muuttujilla, jotka indikoivat maalta peräisin olevia virtoja, auttaisi selvittämään paremmin tulevaisuuden skenaarioita Grönlannin rannikkoalueella.

Avainsanat – Nyckelord – Keywords

Paleoekologia, holoseeni, panssarisiimalevien kystit, C:N, $\delta^{13}C$, $\delta^{15}N$, biogeeninen pii, orgaanisen hiilen kokonaismäärä, Arktinen alue, Koillis-Grönlanti, rannikkoalueet, merijää

Säilytyspaikka - Förvaringsställe - Where deposited

HELDA - Digital Repository of the University of Helsinki

Muita tietoja - Övriga uppgifter - Additional information

Table of contents

1. Introduction

The Arctic is warming twice as fast as the global average with dramatic consequences. Polar areas act like a refrigerator for the rest of the globe with cool air and water masses flowing towards the equator (Pörtner et al., 2019). Under current climate change, this global temperature regulating system is threatened. The Arctic area is particularly sensitive to global warming, as the environment is characterised by ice, snow and permafrost, all of which have been shrinking over the last decades (Overland et al., 2017, Meredith et al., 2019). The melting cryosphere induces sea level rise, changes ocean vertical structure and circulation, and collapses permafrost landscapes, potentially releasing more greenhouse gases to the atmosphere (Arrigo K.R. & van, 2015, AMAP, 2017) These changes are also viciously accelerating each other (Pörtner et al., 2019). One of the most rapid changes in the Arctic is sea-ice retreat (Barber et al., 2017).

Between 1975 and 2012, the thickness of sea ice decreased approximately 65% in the central Arctic Ocean, and since 1979 the Arctic perennial sea ice has decreased almost 50 % in area (Barber et al., 2017, Meredith et al., 2019). It is likely that by the end of the 2030s' the Artic Ocean will be totally ice free during summers (Barber et al., 2017). Longer open water periods increase light and nutrient availability often enhancing net primary production (NPP) and shifting the timing of phytoplankton blooms (Meredith et al., 2019; Ribeiro et al., 2017). In the past two decades, NPP in the Arctic Ocean has increased 30%, but there has been marked regional heterogeneity (Arrigo & van Dijken, 2015, Meredith et al., 2019). Changes in sea-ice cover and primary production affect marine ecosystems by shifting the distribution of species and causing cascading effects in food web structure, with impacts on biodiversity and fisheries (Barber et al., 2017, Meredith et al., 2019). Retreating sea ice increases gas, heat and moisture exchange between the ocean and the atmosphere, amplifying the Arctic hydrological cycle (Bintanja & Selten, 2014). Increasing precipitation on land amplifies river discharge, which will enhance freshwater, sediment and nutrient inputs into the Arctic Ocean (ibid.). This will affect ocean acidification and primary production, change the vertical stratification of the ocean, decrease the ventilation of bottom waters, and even influence hemispheric phenomena such as the Atlantic Meridional Overturning Circulation (AMOC) (Bintanja & Selten, 2014, AMAP, 2017, Meredith et al., 2019).

The freshwater volume in the upper layer of the Arctic Ocean has increased more than 11 % (Prowse et al., 2017). Most of the freshwater input to the Arctic Ocean comes from the melting Greenland

Ice Sheet, which is also the single largest land ice source for sea-level rise (Box et al., 2017). The current rate of ice loss from the Greenland Ice Sheet has more than doubled compared to the rates from 1983–2003 (Kjeldsen et al., 2015), and the average ice loss was approximately 278 Gt per year between 2006 and 2015 (Meredith et al., 2019). The submarine melt rate of Greenland's tidewater glaciers is mostly determined by the temperature of ocean water eddying through Greenland's fjords (Box et al., 2017). The ice loss in Greenland is most accelerated at west coast fjords, which are affected by relatively warm and saline Atlantic waters (Dahl-Jensen et al., 2011, Box et al., 2017), but the freshwater supplies in Northeast Greenland fjord systems and Northeast Greenland coastal waters in general are also increasing (Sejr et al. 2017). Increasing freshwater input to the Greenland Sea could have far-reaching consequences, as it is the Earth's most important deep-water formation region and hence, crucial for global thermohaline circulation (Overland et al., 2017).

Since marine-terminating glaciers in Greenland are retreating and thinning, the relative amount of land-terminating glaciers will increase in the near future (Meire et al., 2017). In Arctic fjords, productivity is significantly influenced by the position of glacier termini (ibid.). Subsurface melt-water plumes from marine-terminating glaciers induce upwelling of macronutrients and dissolved inorganic carbon from the bottom waters to the surface in front of the glacier (Kanna et al., 2018). The upwelling water is a mixture of fresh meltwaters and sea waters, and is highly turbid (ibid). This mechanism sustains high summer phytoplankton productivity in the fjords particularly near the boundary of the surface freshwater layer and the subsurface layer of turbid water (Meire et al., 2017, Kanna et al., 2018). This kind of upwelling is absent in fjords influenced only by land-terminating glaciers and hence, productivity is generally lower (Meire et al., 2017). Surface runoff from the melting of land-terminating glaciers may in fact decrease primary production, as the amount of suspended material in meltwater is high, causing high turbidity and decreasing the availability of light (Murray et al., 2015). In areas without upwelling, increased meltwaters can also amplify stratification, which prevents the utilisation of nutrients from deeper waters (Murray et al., 2015, Meire et al., 2017). As higher productivity in fjords where upwelling takes place also supports fisheries, the melting of Greenland's glaciers near fjords may decrease fish stocks, biodiversity and cause socio-economic impacts (Meire et al., 2017).

The effects of Arctic warming have consequences to latitudes below the Arctic (Pörtner et al., 2019). Understanding the impacts of sea-ice changes, and freshening and warming of the Arctic Ocean on Arctic marine ecosystems and beyond is still limited (Sejr et al., 2017, Pörtner et al., 2019). The

possible consequences of Arctic climate change for coastal ecosystems influenced by changes on land and in the sea are particularly deficiently understood (Heikkilä et al., 2019). Yet Arctic shores sustain high biodiversity and important fisheries, making them socio-economically the most important regions for the Arctic population (AMAP, 2017, Meire et al., 2017). For predicting the ecosystem responses to climate change, it is important to gain reliable information from millennial-scale variability (Ribeiro et al., 2017). Also, for distinguishing the anthropogenic impact on climate from natural variability, it is crucial to put modern climate change into a longer-term context (IPCC, 2007).

1.1. Reconstructing past ocean conditions from marine sediment records

Paleodata are empirical "measurements" of past environmental conditions, e.g. sea ice, temperature and biodiversity, which come from paleoarchives (Ruddiman, 2014 pp. 55–77). Most of the Earth's climate history is recorded in trees, corals, ice and the major climate archive; sedimentary debris accumulated in lake and sea bottoms (Mann, 2002, Ruddiman, 2014 pp. 55–77). Climate archives record a chronologically ordered set of physical, chemical and biological indicators of past environments, i.e. proxies (Mann, 2002). The two most commonly used climate proxy - groups are physical-geochemical proxies (e.g. sediment organic compounds and stable isotopes) and biotic proxies (e.g. diatoms and palynomorphs) (Ruddiman, 2014 pp. 55–77).

Palynomorphs are organic-walled microfossils, 5–500 µm in size, including multiple biological groups (Traverse, 2007). As they are composed of very resistant organic material, they are abundant in most sediment deposits and resistant to routine palynological preparations where calcerous and siliceous componds are removed (ibid.). They include e.g. pollen, spores and remains of various aquatic plankton groups, such as dinoflagellate cysts (ibid.).

Dinoflagellate cysts are commonly used biological proxies for reconstructing past marine environments. Dinoflagellates are microscopic single-celled and motile organisms, found in most types of aquatic environments from the equator to polar areas (Fukuda & Suzaki, 2015, pp. 23–45). Including phototrophic, mixotrophic and heterotrophic species, dinoflagellates are an important part of marine food webs and together with diatoms and coccolithophorids they form the majority of primary producers in the global ocean (de Vernal & Marret, 2007 pp. 371–408). As a part of their life cycle, 10–20 % of dinoflagellate species form a resting cyst, or a dinocyst, typically 15–100 µm in diameter, which enables survival of the cell during a dormancy period (de Vernal & Marret, 2007

pp. 371–408, Mertens et al., 2019). Because of their diverse species composition, dinocysts provide an excellent proxy for reconstructing marine environments, sea surface temperature (SST), sea surface salinity (SSS), sea ice and productivity (de Vernal & Marret, 2007, pp. 371–408; Sherr & Sherr, 2007). As they are made of resistant organic compounds, dinocysts preserve very well in the sediment, and hence they are particularly useful in areas where calcareous foraminifera or siliceous diatom remains are prone to dissolution (de Vernal & Marret, 2007 pp. 371–408). Dinoflagellates are adapted to a wide range of salinities, and hence the species diversity is higher in near-shore areas (ibid.), which makes them particularly good proxies for coastal regions.

Pollen and spores are also commonly used proxies for climate reconstructions. They are widely distributed and preserve well in the sediment (Ruddiman, 2014 pp. 55–77), which makes them an excellent proxy to reconstruct regional vegetation and climate change on the continent . In marine environments, pollen and spores can also be used to detect catchment vegetation change and terrestrial inputs, and increased amounts of pollen from local vegetation can illustrate enhanced river discharge. Other widely used biotic proxies for reconstructing marine environments include diatoms and planktic and benthic foraminifera (Jorissen et al., 2007, pp. 263–325). One quite untraditional way to use benthic foraminifera together with dinocysts, is to calculate the amount of their organic linings found on the same microscope preparations . Calcareous foraminifera dissolve during the dinocyst sample preparation, but as their inner linings do not, they can be used to detect the total amount of foraminifera, which can be used as indirect tracers of productivity (Jorissen et al., 2007, pp. 263–325, Ni Fhlaithearta et al., 2013). Other palynomorphs than can be used together with dinocysts, and hence do not require separate sample preparations include *Hexasterias problematica* and the genus *Halodinium* spp. which have been typically used to to detect freshwater and glacial meltwater inputs (Sorrel et al., 2006, Richefol et al., 2008). Both of them are acritarchs, i.e. palynomorphs for which biological affinities are not known.

In addition to microscopic proxies, geochemical indicators can be used to reconstruct past marine conditions. The sediment total organic carbon (TOC) content describes the amount of organic carbon delivered to the sediment, and hence gives a general estimate of changes in primary production at the study site (Meyers, 1994). The ratio between organic carbon and nitrogen, or C:N value, in the sediment helps distinguishing what proportion of the organic material deposited in the sediments originates from terrestrial or marine sources (Limoges et al., 2018). Due to the absence

of cellulose, algae typically have atomic C:N values between 4–10, as for terrestrial vascular plants C:N ratios rise above 20 (Meyers, 1994). Stable isotopes of e.g. carbon and nitrogen are also widely use proxies in aquatic environments. Stable isotope composition of sedimentary organic carbon ($\delta^{13}C$) can give insight into the source of organic matter (Meyers, 1994,), and e.g. ice algae production in marine environments (Søreide et al., 2006). Stable isotope composition of sedimentary nitrogen ($\delta^{15}N$) can demonstrate the uptake and limitation of nitrate in marine ecosystems (Limoges et al., 2020, Robinson et al., 2021). Highly branches isoprenoid lipids (HBIs) are ice-associated biomarkers used to reconstruct particularly sea ice, as they are biosynthesized by a limited number of diatoms living in sympagic (i.e. ice-associated) environments (Belt, 2018). There are several HBI types, including e.g. source-spesific Ice Proxy with 25 carbon atoms (IP_{25}), which is a direct sea ice proxy (ibid.).

Multiproxy methods, i.e. using more than one line of evidence, are recommended to use for reconstructing the past (Mann, 2002). Environment and climate reconstructions based on one or multiple proxies can be qualitativeor quantitative. Quantitative reconstructions using biological proxies are based on the knowledge of species' modern habitats and their environmental preferences (Ruddimann, 2014 pp. 55–77). Hence, their reliability is highly dependent on the calibration with modern samples. To set the climate records to human time scale, they can be dated with radiometric methods, using for example radiocarbon (^{14}C) (Ruddiman, 2014 pp. 55–77). The ^{14}C dating method is based on the unstable carbon isotope ^{14}C, which is absorbed by living organisms. The half-life of ^{14}C, i.e. the time half of this isotope is decayed from a dead organism, is approximately 5730 ± 40 years (Godwin, 1962) and therefore after approximately 50 000–55 000 years the ^{14}C isotope is decayed completely (Hajdas, 2008). Considering that much of the carbon in marine environments is older than carbon in the atmosphere, it is recommend to use a local marine reservoir correction ΔR when dating remains organisms that absorb most of the carbon from the ocean (Stuiver et al.,1986).

1.2. Holocene climate history in Northeast Greenland

Changes in the Northern Hemisphere summer insolation drove the major changes in climate during the current interglacial, the Holocene (Ruddiman, 2014 pp. 273-294). The Northern Hemisphere insolation was at its highest between 10 000 and 5 000 years before present (BP), which corresponds to the Holocene Thermal Maximum (HTM) when global temperatures were approximately 0.6 °C warmer than the Holocene global average (Marcott et al., 2013). The gradual cooling after 5 000

years BP in the Northern Hemisphere was also linked to orbital forcing (ibid.). There is, however, spatial variability in the temperature anomalies caused by differences in mean annual insolation between polar areas and low latitudes, as well as atmospheric and oceanic feedbacks, including effects from remaining ice sheets (Marcott et al., 2013; Masson-Delmotte et al., 2013). For example in eastern Arctic Canada and Greenland, many records lag peak summer insolation and register HTM sometime between 9000 and 5000 years BP (Briner et al. 2016). In the northern and the eastern Arctic, the temperature records indicate an earlier Holocene warmth period than in the south and the west (ibid.). In Northeast Greenland there is a lack of records and the HTM is not well constrained (ibid.). The East Greenland shore is influenced by the East Greenland current, which is the major southward transportation route for sea ice and cold, low-salinity water masses; most of the water from the Arctic Ocean passes through Fram Strait (Dahl-Jensen et al., 2011). Hence, the climate changes in East Greenland coastal areas do not only indicate local changes but also changes taking place in northern Greenland and in the Arctic Ocean (ibid.).

There are not many detailed marine sediment core records of past sea-ice variation (de Vernal et al., 2013a, de Vernal et al., 2013b), but much positive development has taken place in the recent decade (e.g. Belt, 2018). While only few records have been produced from Northeast Greenland (Ribeiro et al., 2017), the existing data from the region illustrates the following:

Phytoplankton biomarkers, and quantitative reconstructions based on foraminifera and dinocysts indicate relatively warm early Holocene between 10 500 and 9300 years BP with pro-longed open water periods in Fram Strait (Werner et al., 2016, Falardeau et al., 2018, see Fig. 1). Quantitative reconstructions based on dinocyst assemblages from marine sediments in southeastern Greenland illustrate warmer than present conditions between 9000-6000 years BP (Solignac et al., 2006). After approximately 5200 years BP, the foraminifera data from Fram Strait indicate extensive sea-ice cover (Werner et al., 2013, 2016). Also, benthic foraminifera and stable isotope records from marine sediments in eastern Greenland illustrate a shift towards colder and lower-salinity conditions approximately 5000 years BP (Jennings et al., 2002). Lake sediment cores from the coastal area of Northeast Greenland based on e.g. pollen, diatoms and geochemical measurements indicate the Medieval Climate Anomaly around 1 000 years BP, when temperatures generally rose above the long-term average, the Little Ice Age after 800 years BP, when temperatures were below the long-term average, and recent warming approximately over the last 100 years (Wagner et al., 2000, 2008).

The present retreat of the Greenland Ice Sheet will increase the amount of fjords surrounded by only land-terminating glaciers in the future. This will most likely affect the productivity and ecosystem structure of coastal marine areas. Understanding how these changes in glaciers will act together with retreating sea ice, and the freshening and warming ocean will be crucial for understanding Arctic coastal change. Paleorecords enable gathering information of these interactions over past millennia, which can improve our understanding of drivers of Arctic coastal ecosystem change and provide possible future scenarios. At present, there are not many high-resolution marine ecosystem reconstructions from the Arctic near-shore areas, and in particular those, which take into account land-derived inputs are lacking.

1.3. Objectives of the thesis

The main objective of this thesis is to provide a detailed reconstruction of coastal marine ecosystem change over the Holocene in Young Sound fjord, Northeast Greenland. Young Sound is at present surrounded only by land-terminating glaciers, yet there might have been marine terminating glaciers before 9000 years BP (Lecavalier et al., 2014). I studied the linkages of reconstructed ecosystem changes to previous sea-ice and temperature records from Northeast Greenland, and to land-derived freshwater and nutrient inputs reconstructed in this thesis.To detect the ecosystem changes I studied the dinoflagellate cyst species composition from two radiometrically dated cores from Young Sound fjord. Even though dinoflagellates represent only part of the ecosystem, they are one of the main primary producers (de Vernal & Marret, 2007 pp. 371–408) and thus variability in dinocyst concentrations and species composition are likely reflected in the food web. Total organic carbon %(TOC%), total nitrogen (TN%), biogenic silica (BSi), and stable isotope of nitrogen ($\delta^{15}N$) from the same cores were examined in order to analyse the fjord's productivity during the Holocene. As the fjord is affected by the East Greenland Current (EGC) (Sejr et al. 2017), the sediment archives can also record regional climate and oceanographic changes in northern and eastern Greenland and in the Arctic Ocean. To distinguish whether the possible freshwater input is local, i.e. melting from the glaciers near Young Sound, pollen and spore assemblages, carbon to nitrogen ratio (C:N), and carbon stable isotopic compostion ($\delta^{13}C$) were analysed. The hypotheses are:

1. The changes in ecosystem structure follow the Holocene climate and sea-ice variability in the region (e.g. Solignac et al., 2006, Müller et al., 2012, de Vernal et al., 2013c, Werner et al., 2013, 2016, Syring et al., 2020).

2. Local melting, i.e. terrestrial freshwater input, affects the ecosystem structure and productivity in the fjord system.

The new information of past ecosystems and productivity in the Arctic coastal areas produced in this thesis is crucial for predicting future responses along the Arctic shores. The results can also help to improve the use of proxies in Arctic coastal areas, and provide insight into future marine food-web structures, which affect the social and economic possibilities of Arctic people.

2. Materials and methods

2.1. Regional setting

Young Sound is the outer part of the ca. 90 kilometres long Young Sound-Tyrolerfjord system in Northeast Greenland (74° N 20° W) (Fig. 1). The fjord is affected by several rivers and land-terminating glaciers within the catchment, but there are no marine-terminating glaciers (Meire et al., 2017; Sejr et al., 2017). In addition to runoff from land, the freshwater input to Young Sound-Tyrolerfjord originates from precipitation, melting of sea ice, the Greenland Ice Sheet and freshwater input from the Arctic Ocean transported by the East Greenland Current (Sejr et al., 2017). The shallow sill at ca. 45 m of water depth prevents the dense Atlantic water entering the fjord (ibid.) (Fig. 2). The ice-cover duration in Young Sound is ca. 9 months (Ribeiro et al., 2017; Sejr et al., 2017). During summers, glacially derived particles cause high turbidity, which limits the light penetration and primary production in the fjord system (Meire et al., 2017; Ribeiro et al., 2017). The nitrate concentration of the riverine meltwater is low, which is also the case in the surface water layer of the fjord (Meire et al., 2017).

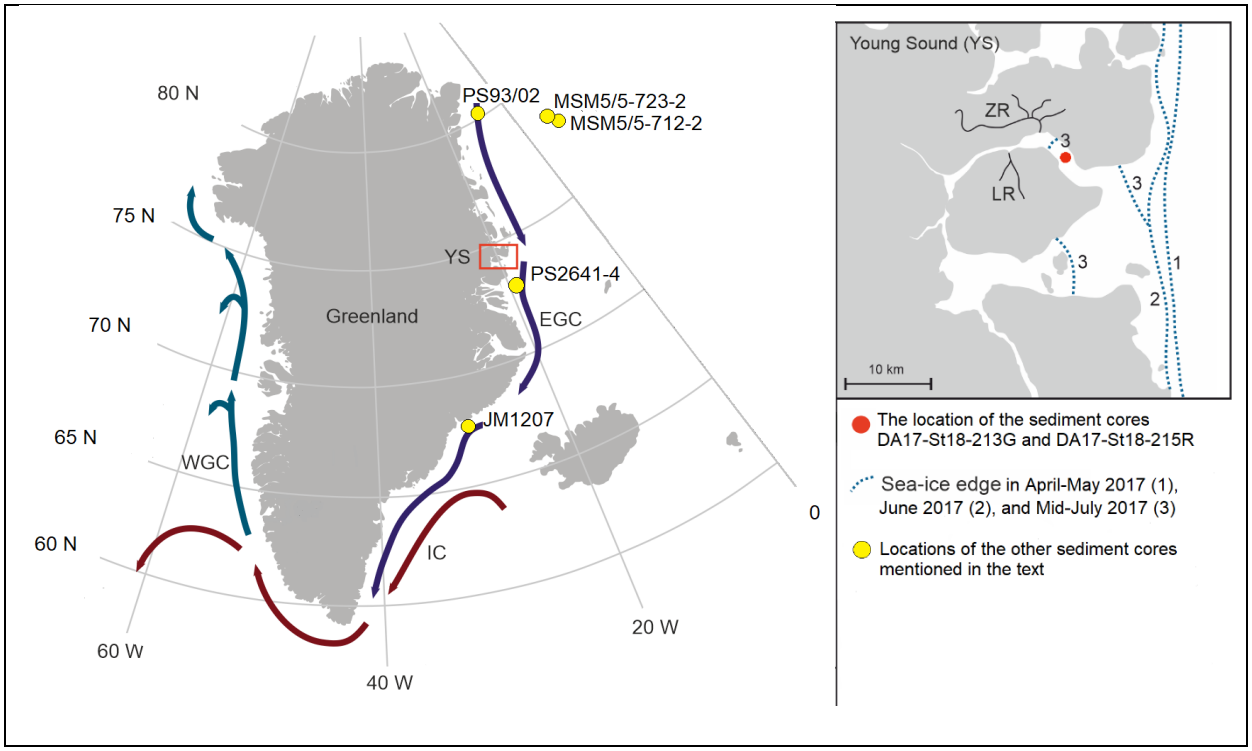

Figure 1. Map of Greenland with blue arrows indicating the East Greenland Current, light blue arrows indicating the route of the West Greenland Current and red arrows indicating the Irminger Current. The location of the Young Sound-Tyrolerfjord systems is indicated with by a red square, and the study site is marked with a red circle in the smaller map. Also, the main rivers near the site (Lerbugt River, and Zackenberg River) are indicated on the map. Blue dotted lines indicate sea-ice edge in (1) April-May, (2) June, and (3)

Mid-July, 2017. Yellow circles indicate the other sediment cores mentioned in the text: JM1207 (Solignac et al., 2006), PS2641-4 (Müller et al., 2012), PS93/02 (Syring et al., 2020)., MSM5/5-723-2 (Werner et al, 2016), MSM5/5-712-2 (Müller et al., 2012, Werner et al., 2013, de Vernal et al., 2013c).

Stratification caused by meltwaters impedes nutrient supply from deep waters, restricting phytoplankton biomass to the deeper parts of the water column after the surface water has been depleted in nutrients (Meire et al., 2017; Sejr et al., 2017). The overall pelagic primary production in Young Sound is low, ca. 10 g C m^{-2} yr^{-1} (Rysgaard et al., 1999; Meire et al., 2017). The phytoplankton community includes diatoms, dinoflagellates, silicoflagellates, ciliates, chryosphytes, heliozoans and radiolarians, with diatoms dominating the community (Rysgaard et al., 1999; Krawczyk et al., 2015).

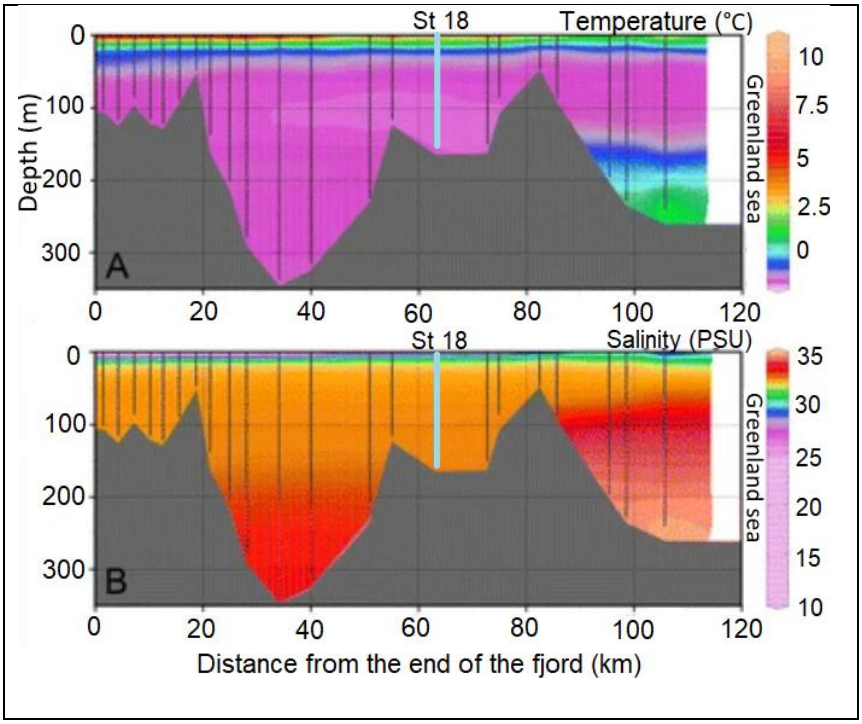

Figure 2. Topography of the Young Sound fjordsystem, and A) temperature (Celsius degrees), and B) salinity (PSU, practical salinity unit, g/kg) along the fjord in early august 2014. Light blue lines indicate the study site. Modified from Ribeiro et al. (2017).

2.2. Field sampling

The two sediment cores used in this study were collected in September 2017 from the NorthGreen 2017 research vessel R/V Dana (Seidenkrantz et al., 2017). One ca. 91 cm long Rumohr-lot core, DA17-St18-215R, and one ca. 310 cm piston gravity core, DA17-St18-213G, were collected from the mouth of Young Sound (74°20'55.68" N, 20°20'13.74" W) at the depth of ca. 168,2 m (Ibid.). DA17-

St18-215R is here called Rumohr core and DA17-St18-213G gravity core. A gravity corer can disturb and compress the surface sediment when penetrating the seafloor and to get better preserved surface sediment samples a Rumohr corer is often use together with a gravity corer. The Rumohr core was split and subsampled on board at every 0,5 cm and the gravity core was cut into sections of 1 m and stored in a cooling room. Both cores were sent to the Geological Survey of Denmark and Greenland (GEUS).

2.3. Geochronology

Six radiocarbon dates were used for the age-depth model from the Rumohr core and five from the gravity core, respectively (See Table 1.) (Nygaard Eriksen 2018; Bang Kvorning, 2020, pp. 15-19). Bivalve shells (*Nucula* species, *Thyasira gouldi*, *Ennucula tenuis, Yoldiella intermedia*, *Axinopsida orbiculata* and unidentified shell fragments) were used for ^{14}C dating for both cores. Radiocarbon dating was performed at the Aarhus AMS Centre, Department of Physics and Astronomy, Denmark by using Accelerator Mass Spectrometry (AMS). From the Rumohr core, two dates were measured at the Laboratory for Ion Beam Physics, EHT Zurich by using a new method described in Bard et al., 2015 and Wacker et al., 2013. There, small amounts of carbonate are analysed directly in a combat AMS facility equipped with a gas ion source (Table 1, blue lines). The Rumohr core was also tested for ^{210}Pb activity using gamma-spectrometry at the Gamma Dating Centre, Department of Geography and Geology, University of Copenhagen. ^{210}Pb was analysed for the first approximately 10 cm of the Rumohr core and ages calculated using the Constant Rate of Supply (CRS) model (Andersen, 2017).

Table 1. Overview of radiocarbon dates, cal Years BP (calendar years before present) and calibrated age ranges. Blue colour refers to Accelerator Mass Spectrometry (AMS) facility equipped with gas ion source, white colour refers to AMS ^{14}C dating method.

Core	Depth cm	Material	^{14}C age (cal Years BP)	^{14}C age (+/- years)	Min. (cal Years BP)	Max. (cal Years BP)	Median (cal Years BP)
215R	10.5	Shell (*Nucula* sp.)	664	31	90	114	117
215R	18.5	Shell (*Thyasira gouldi*)	938	26	290	497	403
215R	24.5	Shell fragments	1170	60	485	714	587
215R	67.5	Shell fragments	2855	60	1949	2288	2138

215R	74.5	Shell (*Thyasira gouldi*)	2642	24	2104	2384	2243
215R	80.5	Shell (*Thyasira gouldi*)	2763	31	2209	2565	2348
213G	31.5	Shell fragments	2072	32	1284	1563	1432
213G	45	Shell (*Ennucula tenuis*)	2358	23	1683	1928	1810
213G	57	Shell (*Ennucula tenuis*)	2657	23	2033	2304	2170
213G	81.5	Shell (*Axinopsida orbiculata*)	3463	47	2860	3318	3097
213G	225	Shell (*Yoldiella intermedia*)	7723	33	7707	8257	8048

The age-depth models were constructed with the program 'R' using the BACON package, based on Bayesian accumulation model code with probability intervals of 95% (Blaauw & Christen, 2011). The ^{14}C dates were calibrated using the Marine13 radiocarbon calibration curve (Reimer et al., 2013) and a local reservoir correction (ΔR) of 140 ±60 (Blaauw & Christen, 2011) for the Rumohr core and 161 ±24 for the gravity core (Håkansson, 1973 cited in Nygaard Eriksen, 2018, Stuiver et al., 2018 cited in Nygaard Eriksen, 2018,). The surface of the gravity core was assumed to be of modern age. The sedimentation rate for both cores, over time covered in by the age model, was calculated using the following formula:

$$Sedimentation\ rate = \frac{Depth_{bottom} - Depth_{top}}{Age_{bottom} - Age_{top}}$$

Where depth refers to the cm depth of the investigated interval from the bottom to the top, and age refers to the calibrated years BP for the interval. This is an average sedimentation rate over the time of investigated intervals, and even though the sedimentation rate has likely not been stable over time, it will give an insight of the general sedimentation rate.

2.4. Dinoflagellate cysts and other palynomorphs sample preparation and identification

Samples for palynological analysis were prepared following the method described in Quaijtaal et al. (2014) at GEUS Copenhagen (Rumohr core) and Ghent University, Belgium (piston gravity core). The Rumohr core was analysed for palynomorphs at every 5 cm between 20–73 cm and at a 10 cm

resolution between 73 and 90 cm. The gravity core was analysed at every 10 cm. The samples were oven-dried at 60 °C, weighed and rehydrated with demineralised water. For estimating the absolute dinocyst concentrations, one tablet containing 10 000 *Lycopodium clavatum* spores was added to each 0.8–3.2 g sediment sample before treatment (Stockmarr, 1971). Rumohr core sediment samples were soaked in 2 N hydrochloric acid (HCl) for a day, 40 % hydrofluoric acid (HF) for two days and again in 2 N HCl a day to remove calcium carbonate and silicates. Gravity core sediment samples were repeatedly treated with 2N HCl and 40 % HF. Both cores' samples were rinsed with distilled or deionized water. The residues were sonicated for 30 seconds to break the organic matrix and sieved through a 11 µm nylon mesh (Rumohr core samples) or through 10 µm nylon mesh (gravity core samples) to remove fine particles. The homogenised residue was mounted with glycerine jelly on a microscope slide and topped with a cover slip.

Dinoflagellate cysts and pollen, spores and other palynomorphs were identified using a Zeiss Imager A2 light microscope with 60x oil immersion objective. The dinocyst identification was based on morphological characteristics, i.e. shape, ornamentation and colour of the cyst, cyst wall structure, and type and size of possible archeopyle and processes. Photographs were taken with a Zeiss Axiocam 506 color camera. Due to low concentrations of dinocysts, a minimum of 100 cyst were identified per slide. The identification was based on Zonneveld and Pospelova (2015), Liu et al., (2015), Radi et al., (2013), Kawami et al., (2009) and Potvin et al., (2018). The identification of pollen and spores was based on Heikkilä (2001), and the identification for other palynomorphs was based on Bérard-Therriault et al., (1999). Dinoflagellate cysts were identified to species level except when it was not possible because of e.g. folding of the cyst or morphological similarities. Some taxa were grouped for numerical analyses. *Spiniferites* spp. (species) includes all *Spiniferites* specimens which could not be identified as *S. elongatus*, *S. ramosus* or *S. frigidus*. *Brigantedinium* spp. includes all *Brigantedinium* specimens where archeopyle were not observed and therefore could not be identified as *Brigantedinium simplex*, even though it is likely that all do correspond to *B. simplex* in the Young Sound system. *Islandinium minutum* sp. (subspecies) *barbatum* is presented in Potvin et al., (2018) with barbs projected on some of the processes. The barbs are under 0.5-µm long and not always visible with 60x objective. Cysts that were identified as *Islandinium minutum* sp. *barbatum* but where processes did not show barbs are grouped as *I. minutum* sp. *barbatum* no barbs. Sea-surface salinity and temperature have been related to changes in morphology of dinoflagellate cysts (e.g. Ellegaard et al., 2002; Verleye et al., 2012, Jansson et al., 2014). In the North Atlantic Ocean,

salinity is the most important factor affecting the morphology of *Operculodinium centrocarpum*, shorter processes indicating lower salinity and longer processes higher salinity (Jansson et al., 2014). *O. centrocarpum* with short processes (process length 2–5 µm) and with no processes (processes < 2 µm) were separated from *O. centrocarpum* (processes > 5 µm). Because of differing research histories in paleontology and biology, two originally independent taxonomic systems have been developed for dinoflagellates in general, and hence the cyst nomenclatures differ from each other (Elbrachter et al., 2008). The cyst names (paleontological names) and the dinoflagellate (biological) names for the taxa found in this study are presented in table 2.

The concentration (cysts g^{-1} dry sediment) and the abundance of other palynomorphs were calculated according to Stockmarr (1971) using the following formula:

$$dinocyst/dry\ sediment\ weight\ (g) = \frac{number\ of\ cysts\ counted\ x\ number\ of\ Lycopodium\ spores\ added}{number\ of\ Lycopodium\ spores\ counted\ x\ weight\ of\ dry\ sediment(g)}$$

The following formula was used to determine the dinocyst fluxes:

$$Flux\ (dinocycts/cm^2/year) = Sedimentation\ rate\ (cm/year)\ x\ Concentration\ (dinocysts/cm^3)$$

2.5. Geochemical analyses

The organic carbon and nitrogen contents, stable carbon and nitrogen isotope compositions and biogenic silica measurements were conducted at GEOCENTER, Denmark. The total organic carbon (TOC) and total nitrogen (TN) were determined following the method described in Kuzyk et al., (2010). For TOC analysis the samples were treated with HCl for 24 h to remove inorganic carbon. Residues were rinsed with distilled water until the pH reached that of the distilled water. A known amount of material (0.4–2.0g) was packed into tin capsules. Elemental analysis was carried out using a CS-200 LECO or CE 1110 instrument. They were calibrated with a control standard and a blank standard for every 10 samples. For determining $\delta^{13}C$ homogenized samples were treated with 10 % HCl and analysed with a Thermo delta V Advantage isotope ratio mass spectrometer. Untreated subsamples were used to determine stable nitrogen isotopes ($\delta^{15}N$) also with a Thermo delta V Advantage isotope ratio mass spectrometer. Every sample's isotope ratio is expressed as δ-value (‰-deviations from standard) using the following formula:

$$\delta(‰) = 1000\ x\ \frac{R_{sa}-R_{Std}}{R_{Std}},$$

where *R* is $^{13}C/^{12}C$ or $^{15}N/^{14}N$, *sa* is an abbreviation for sample and *std* for standard. Marine limestone, Vienna Pee Dee Belemite (VPDB) was used as a primary standard for carbon and atmospheric air (AIR*)* as a primary standard for nitrogen.

Biogenic silica (BSi) concentrations were determined following the standard method described in DeMaster et al. (1981) at the University of Helsinki (Rumohr core) and GEUS, Copenhagen (gravity core). Weighted amounts of dry sediment were bleached with 1% sodium carbonate (NA_2CO_3) in bottles in a 85 °C water bath. Dissolved silica concentrations were analysed from 1 ml subsamples after 3-, 4- and 5-hour treatments by molybdate blue spectrophotometry. Biogenic silica concentrations were calculated from the measured results with a linear regression equation comparing the increase in silica concentrations against time.

2.6. Statistical analyses

Multivariate ordination methods were used to summarise the principal patterns in the distribution of dinoflagellate cysts, and to approximate the covariances between dinocyst species composition and measured geochemical variables (TOC%, carbon accumulation rates, C:N, BSi, $\delta^{13}C$ and $\delta^{15}N$). Multivariate ordination methods are based on the similarity or distance of the data, and by rearranging the data points concentrated on principal axes, they can reveal major directions of variation in the data and the relation of variables to each other (Shi, 1993). First, detrended correspondence analysis (DCA) was conducted to check whether the sample range has a unimodal or linear distribution. Linear models, such as the Principal Components Analysis (PCA) or the Redundancy Analysis (RDA), should generally be used when species linearly respond to environmental gradients (Ramette, 2007). Although species generally display nonlinear responses to environmental variables, and the response often follows unimodal and in some cases bimodal curves (ter Braak & Looman, 1995a, pp. 29–77), when the samples cover only a short part of the gradient, linear models are recommended (ter Braak, 1995b, pp. 91–173). Gradient length is measured as s.d. units along the first ordination axis. If the length of the axis is less than approximately 2 s.d. (ibid.) linear models can be used. DCA for dinocyst data was conducted using CANOCO 5 (ter Braak & Smilauer, 2002). The length of the axis was 1.15 s.d. units, and hence PCA for dinocyst data was conducted using the C2 programme (Juggins, 2007) and RDA for dinocyst and

geochemical data was conducted using the Past program version 4.05 (Hammer et al., 2001). For both analyses, dinocyst assemblage data were square-root-transformed relative species abundances (√%), and for RDA, the geochemical variables were standardized to make them comparable (ter Braak, 1995b, pp. 91–173).

3. Results

3.1. Geochronology

The chronology of the Rumohr core DA17-St18-215R is based on a combination of ^{210}Pb measurements (first approximately 10 cm, n = 9) and ^{14}C measurements (10.5 – 80.5 cm, n = 6). The chronology of the gravity core DA17-St18-213G is based only on ^{14}C measurements (n = 5). The Rumohr core covers the period from -2 years BP (± 6 years) to 2838 years BP (± 717 years) (Bang Kvorning, 2020, pp. 19–20). The chronology of the Rumohr core is presented in figure 3. The gravity core covers the period of -8 years (± 304 years) BP to 11 510 years BP (± 1 672 years). The chronology of the gravity core is presented in figure 3. The average sedimentation rate was 0.032 cm yr^{-1} in the Rumohr core and 0.025 cm yr^{-1} in the gravity core.

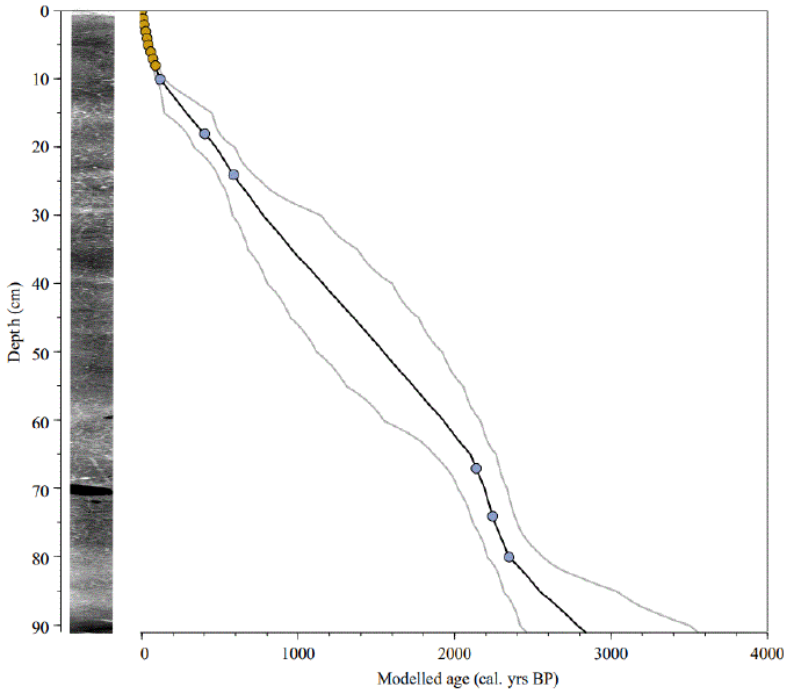

Figure 3. Age-depth model and radiographic x-ray image of the Rumohr core DA17-St18-215R. The age-depth model is based on a combination of ^{210}Pb shown with orange circles and ^{14}C shown with blue circles. The black line indicates the median modelled age-depth relationship and the grey lines indicate minimum and maximum modelled ages in the 95% confidence interval. (Bang Kvorning, 2020, pp. 20).

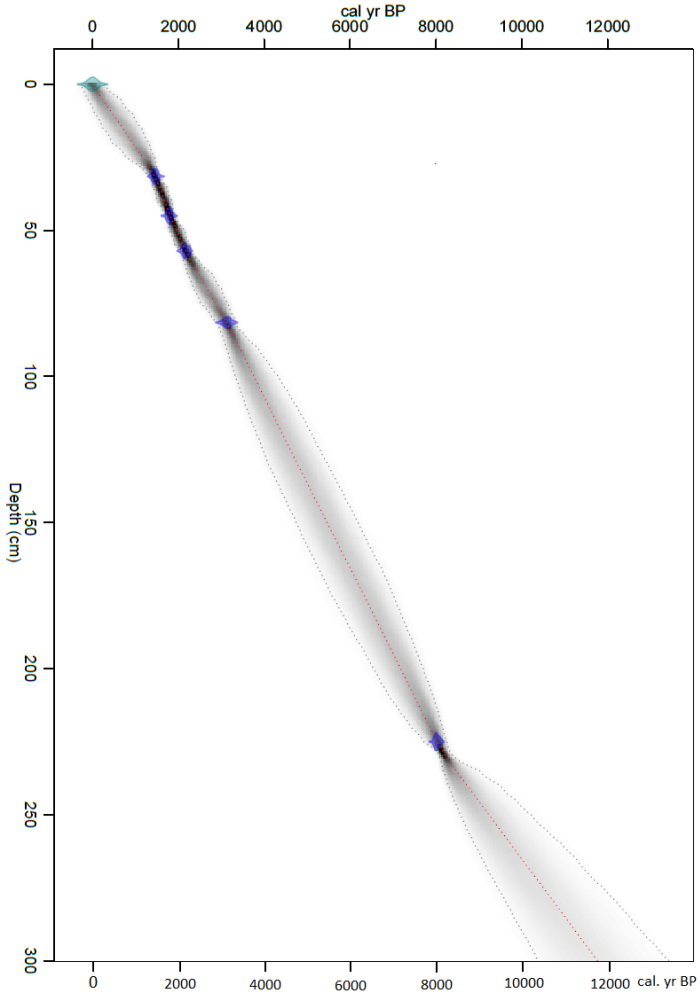

Figure 4. Age-depth model of the gravity core DA17-St18-213G. The age-depth model is based on ^{14}C measurements shown with blue dots. The red line in the middle indicates the mean modelled age-depth relationship and the grey lines indicate minimum and maximum modelled ages in the 95% confidence interval.

As seen in figures 3 and 4, and in Table 1, the modelled ages do not match with the ^{14}C measurements. Also, there is for example an approximately 700 years age difference in ^{14}C results between the cores at 80.5 cm core depth in the Rumohr core and at 81.5 cm core depth in the gravity core (see Table 1), and hence the age models do not correspond with each other either. Based on the age models it is not possible to distinguish which one is more reliable. Between the cores, there seems to be roughly a 10 to 20 cm difference in core depth compared to modelled ages. For example, the median modelled age in the Rumohr core at 67.5 cm core depth is 2138 years, when the median modelled age for the gravity core at 57 cm is 2170 years (see Table 1). As stated in chapter 2.2, the gravity corer can disturb and compress the surface sediment when penetrating the seafloor. However, loss of the surface sediment was not reported (Seidenkrantz et al., 2017).

3.2. Dinoflagellate cysts and other palynomorphs

Dinoflagellate cyst taxa were studied from 20–90 cm core depth, i.e. ~ 470–2800 cal. years BP in the Rumohr core (Fig. 4) and from 0–290 cm core depth, i.e. ~ -8–11 500 cal. years BP in the gravity core (Fig. 5). Sixteen dinocyst taxa that were identified from the samples and their motile counterparts are presented in Table 2.

Table 2. Dinoflagellate cyst taxa identified in this study and their motile forms.

Cyst name (Paleontological)	Dinoflagellate name (biological)
Phototrophic taxa	
cf. *Biecheleria*	*Biecheleria* sp. Indetermined (indet)
Bitectatodinium tepikiense Dale, 1976	cf. *Gonyaulax* spp.
Operculodinium centrocarpum Wall & Dale, 1967 *Operculodinium centrocarpum short processes* *Operculodinium centrocarpum no processes*	*Protoceratium reticulatum* (Claparède & Lachmann) Bütschli
Biological species name used for cyst taxa	Pentapharsodinium dalei Indelicato & Loeblich III
Biological species name used for cyst taxa	Polarella glacialis Montresor, Procaccini & Stoecker
Spiniferites elongatus Reid, 1974	*Gonyaulax elongata* (Reid) Ellegaard, Daugbjerg, Rochon, J. Lewis & Harding
Spiniferites ramosus (Ehrenberg, 1838) Mantell, 1854	*Gonyaulax* cf. *spinifera* (Claparède and Lachmann) Diesing
Spiniferites spp. Mantell, 1850, emend. *Sarjeant, 1970*	*Gonyaulax* spp.
Heterotrophic taxa	
Brigantedinium simplex (Wall, 1967) *ex Lentin and Williams, 1993*	*Protoperidinium conicoides* (Paulsen) Balech
Brigantedinium spp. Reid, 1977 *ex Lentin and Williams, 1993*	*Protoperidinium* spp.
Echinidinium karaense Head et al., 2001	Diplopsalid or Protoperidinoid group
cf. *Diplopsalis* spp.	Unknown
Islandinium brevispinosum Pospelova *and Head, 2002*	*Protoperidinium* sp. indet

Islandinium? *cezare*	*Protoperidinium* sp. indet
Islandinium minutum	*Protoperidinium* sp. indet
Islandinium sp. *barbatum*	*Protoperidinium* sp. indet
Polykrikos quadratus Kunz-Pirrung, 1998	*Polykrikos* sp. indet
Biological species name used for cyst taxa	*Protoperidinium americanum* (Gran & Braarud) Balech

The assemblages were dominated by heterotrophic taxa, particularly *Islandinium minutum* (10–66% percent of the total dinocyst taxa), *Brigantedinium* spp. (4–45%), and *Echinidinium karaense* (7–3%). Accessory heterotrophic taxa consisted of *Islandinium*? *cezare* (0–2%), *Islandinium brevispinosum* (0–3, %), *Islandinium* sp. *barbatum* (0–2%), cf. (confer) *Diplopsalis* spp. (0–7%), *Protoperidinium americanum* cysts (0–2%), and *Polykrikos quadratus* (0–3%). The phototrophic taxa consisted of *Operculodinium centrocarpum* (0-20%), and the occasional occurrence of *Spiniferites elongatus* (0–8%), *Spiniferites* spp. (0–6%), *Spiniferites ramosus* (0–2%), *Pentapharsodinium dalei* cysts (0–6%), *Polarella glacialis* cysts (0–4%), cf. *Biecheleria* cysts (0–4%), and *Bitectatodinium tepikiense* (0–4%). Selected dinoflagellate cyst taxa and other palynomorphs are presented in plates I–III.

The relative abundances of dinocyst taxa and cyst concentrations are presented in Figures 5 and 6. Dinocysts were observed throughout the cores, concentrations ranging between 600 and 11 000 cysts g^{-1} dry sediment (Figs. 5 and 7). The lowest concentrations were found in the lowermost centimetres of the gravity core (290 cm), i.e. around 11 500 years BP. Between 30 and 180 cm core depth, i.e. approximately 6500–1500 years BP, there is a lot variability in the dinocyst concentrations in the gravity core, and a clear peak at 150 cm, i.e. approximately 5500 years BP. Highest concentrations were found from the Rumohr core's sediment samples at 45 cm core depth, i.e. around 1000–1100 years BP. The cyst concentrations show a lot of variability throughout the Rumohr core, but there are three clear peaks at 65 cm, 45 cm, and 29 cm core depth (i.e. around 2100, 1400, and 800 years BP, respectively). However, these peaks are not visible in the gravity core. There is, however, a peak of cyst abundance at 45 cm core depth, i.e. around 1700 years BP. As mentioned before, the concentrations of dinocysts are based on the *Lycopodium clavatum* spores, which were added to the samples before the treatment with HCl and HF, and sieving. It is possible that some of the *Lycopodium clavatum* spores are lost during the preparation process, particularly if they are added to the samples before the treatment (Mertens et al., 2009, 2012). Yet in this case, the low cyst concentrations in both cores may also have influenced to the variability in dinocyst

concentrations due to wider confidence intervals. The dinocyst accumulation follows quite strictly the dinocyst concentration in both cores (Figs. 5 and 7), except for relatively high number of cysts (/g/cm^2/yr) in the bottom part of the gravity core.

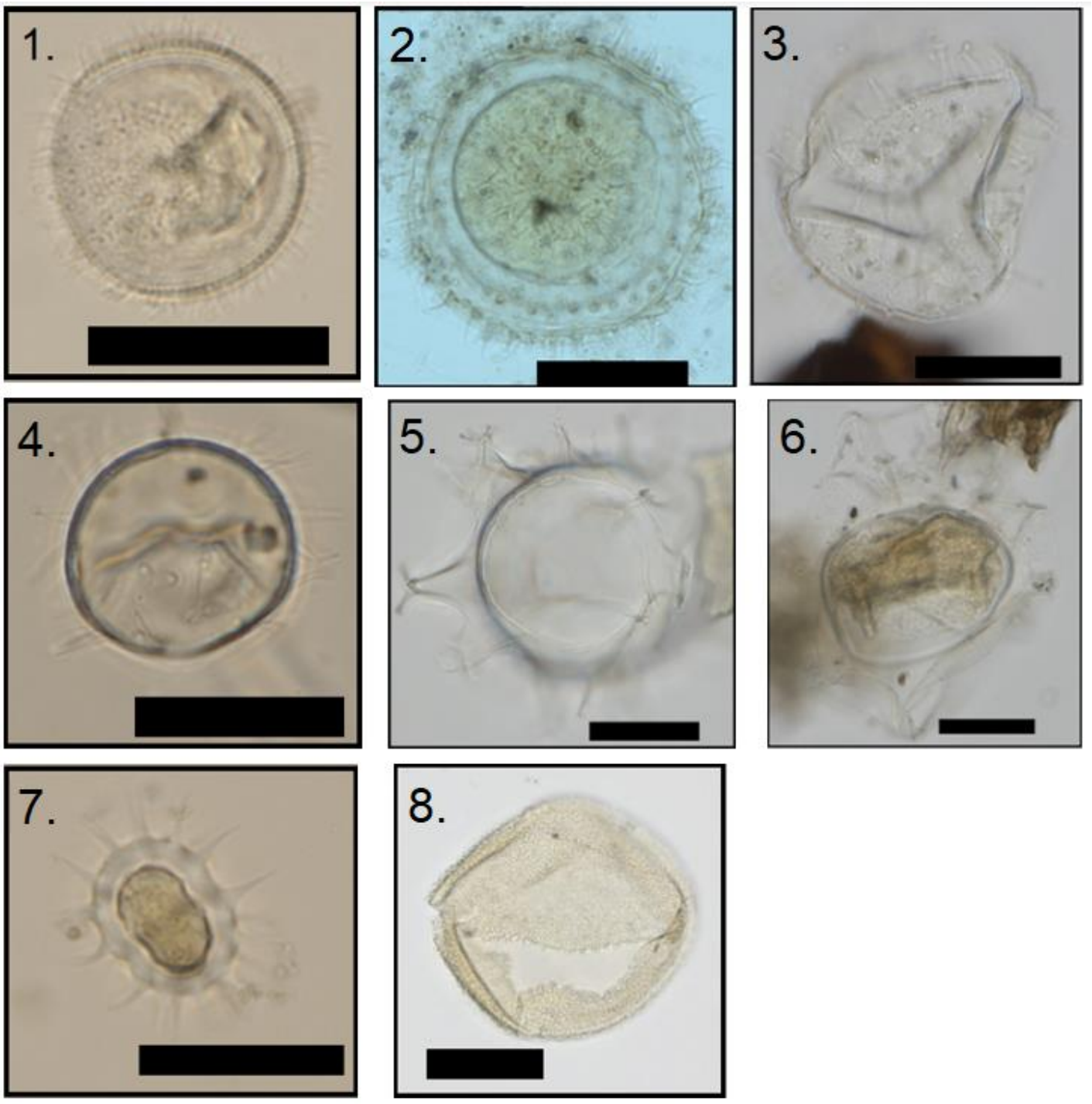

Plate I. Photomicrographs of selected dinoflagellate cysts observed in the cores DA17-St18-213G and -215R taken with a Zeiss Axiocam 506 color camera using a 60 x oil immersion objective: (1) cf. *Biecheleria*, (2-3) *Operculodinium centrocarpum*, (4) *Pentapharsodinium dalei*, (5) *Spiniferites ramosus*, (6) *Spiniferites elongatus*, (7) *Polarella glacialis*, (8) *Bitectotedinium tepikiense*. The black scale bar is 20 µm.

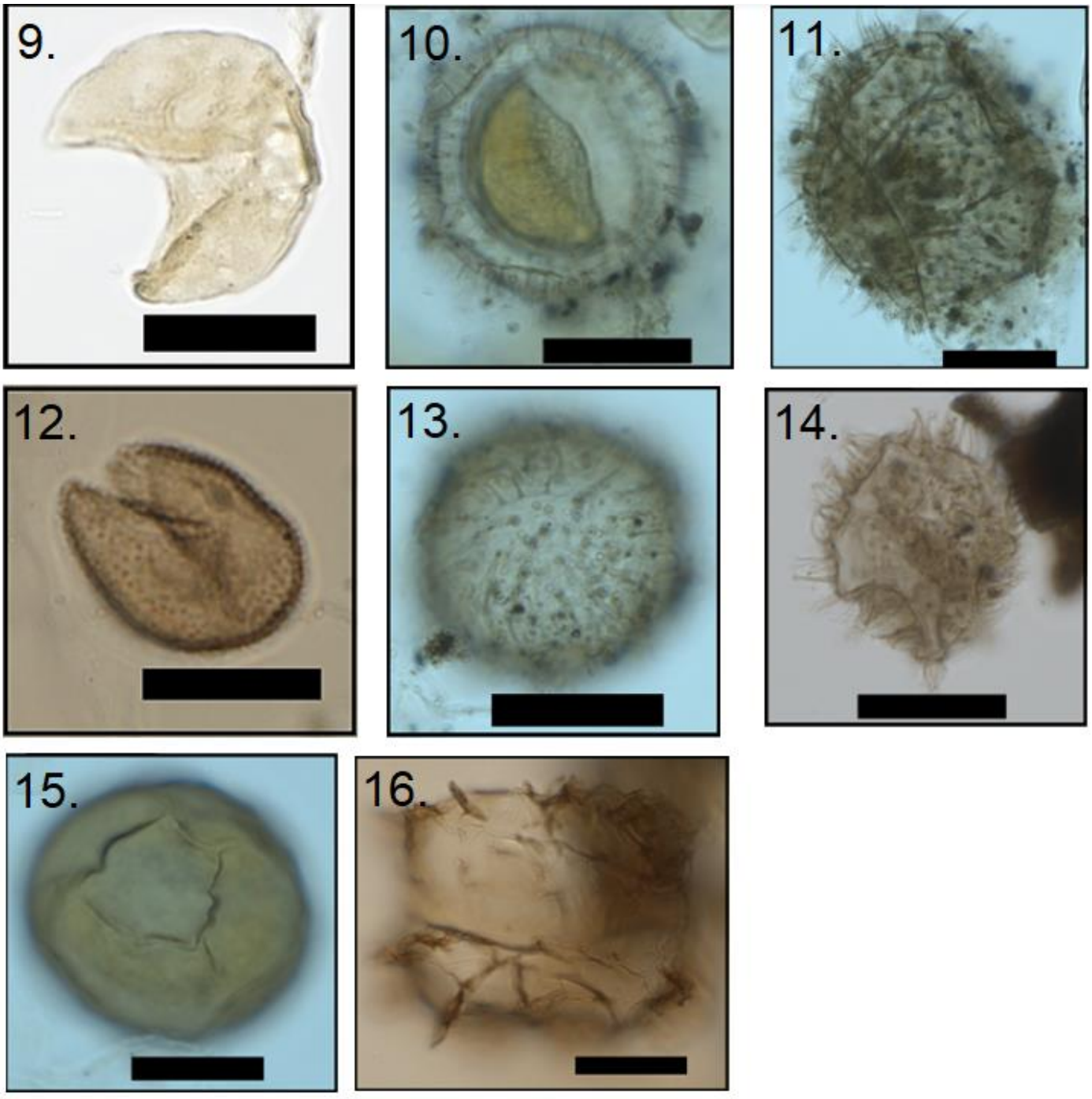

Plate II. Photomicrographs of selected dinoflagellate cysts observed in the cores DA17-St18-213G and -215R taken with a Zeiss Axiocam 506 color camera using a 60 x oil immersion objective: (9) cf. *Diplopsalis* spp., (10-11) *Islandinium minutum*, (12) *Islandinium brevispinosum*, (13) *Islandinium*? *cezare*, (14) *Echinidinium karaense* (15) *Brigantedinium simplex*, (16) *Polykrikos quadratus*. The black scale bar is 20 µm.

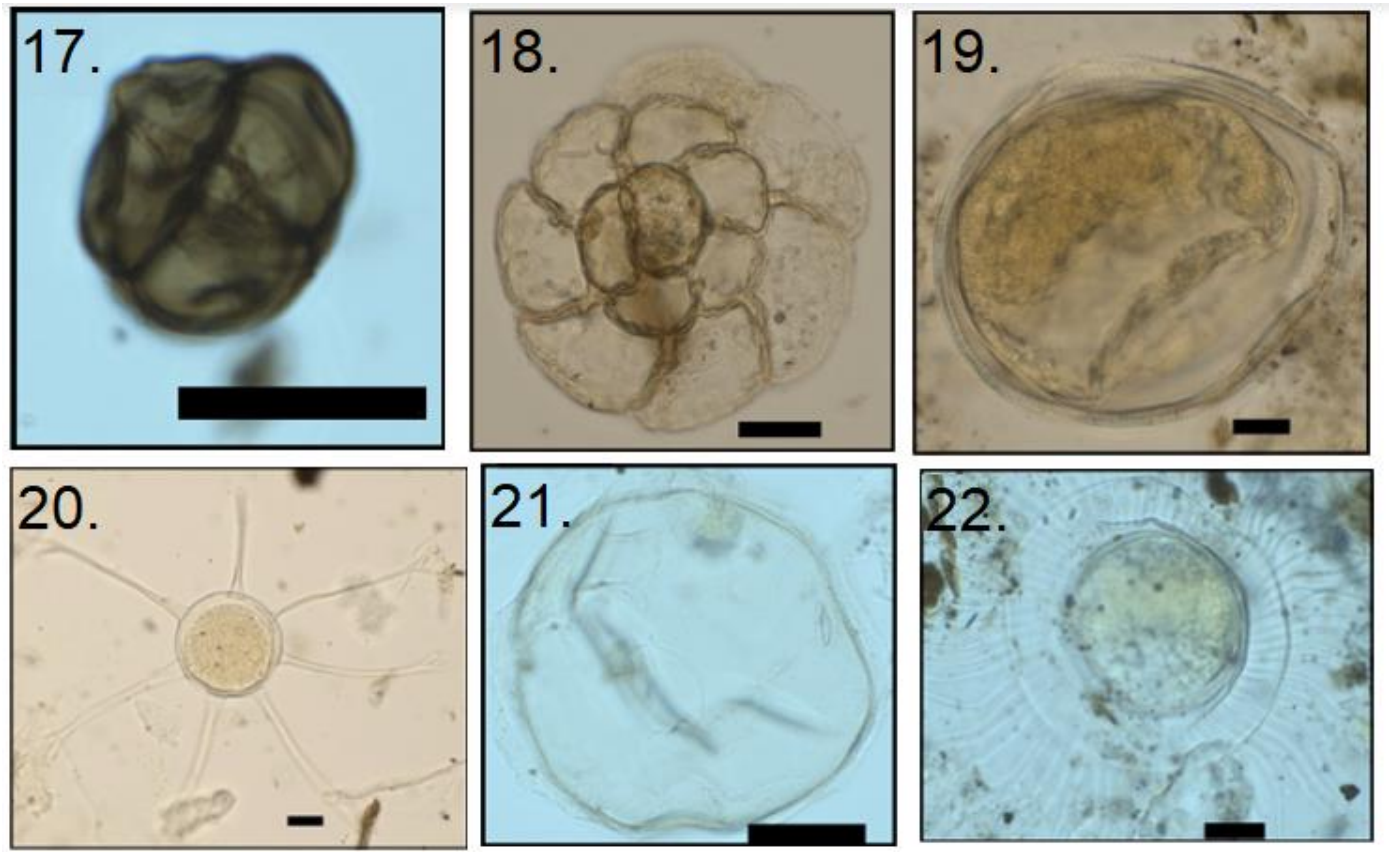

Plate III. Photomicrographs of selected palynomorphs observed in the cores DA17-St18-213G and -215R taken with a Zeiss Axiocam 506 color camera using a 60 x oil immersion objective: (17) Ericaceae pollen, (18) Foraminiferal linings, (19) Copepod egg, (20) *Hexasterias problematica*, (21) *Halodinium* spp., (22) *Radiosperma corbiferum*. The black scale bar is 20 µm.

As the preparation of Rumohr core samples and gravity core samples was carried out in different laboratories (GEUS, Copenhagen and Ghent University, Belgium, respectively) the concentrations between the cores may not be entirely comparable (Merterns et al., 2009, 2012). However, the increasing and decreasing trends of dinocysts in both cores give valuable insight into possible changes in the ecosystem productivity.

There is a clear distinction in the dinocyst taxa between the bottom, middle, and top of the gravity core (Fig. 5). The bottom part of the core, approximately from 290 to 245 cm core depth, i.e. roughly between 11 500 and 9000 years BP, is characterized by rare observations of phototrophic taxa (except for *Operculodinium centrocarpum*), and relatively low abundances of *Brigantedinium* spp. and *Islandinium*? *cezare*. *Islandininium minutum* and *Echinidinium karaense* clearly dominate the dinocyst assemblages.In the middle of the core from 245 to 90 cm, i.e. roughly between 9000 and 3300 years BP, the relative amount of phototrophic taxa increases. *Operculodinium centrocarpum* with short processes or no processes, as well as heterotrophic *Islandinium*? *cezare* are also most

abundant in this section, although the latter is rare between 180–120 cm core depth, i.e. roughly around 6500–4500 years BP. In addition to these two taxa, the middle part of the core is characterized by enhanced variability in the relative amounts of *I. minutum*, *Brigantedinium* spp. and *E. karaense*, particularly between 150–90 cm, i.e. 5500–3300 years BP. At 135 cm core depth, i.e. approximately 5000 years BP, the amount of *I. minutum* is at the lowest level and *O. centrocarpum* at the highest level for the whole Holocene. At the same time, there is a clear increase in the relative abundance of *Brigantedinium* spp. and a decrease of *E. karaense.*

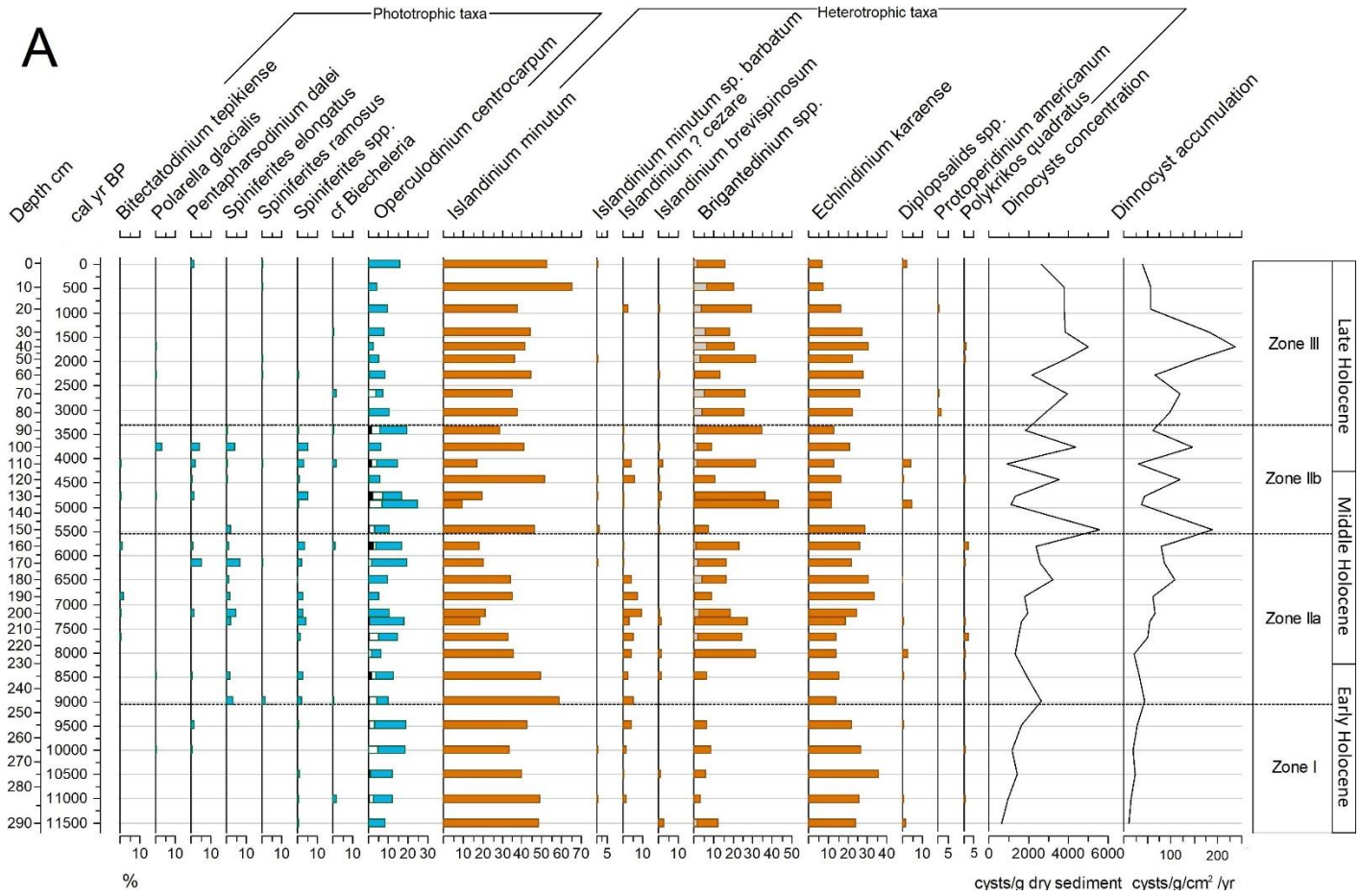

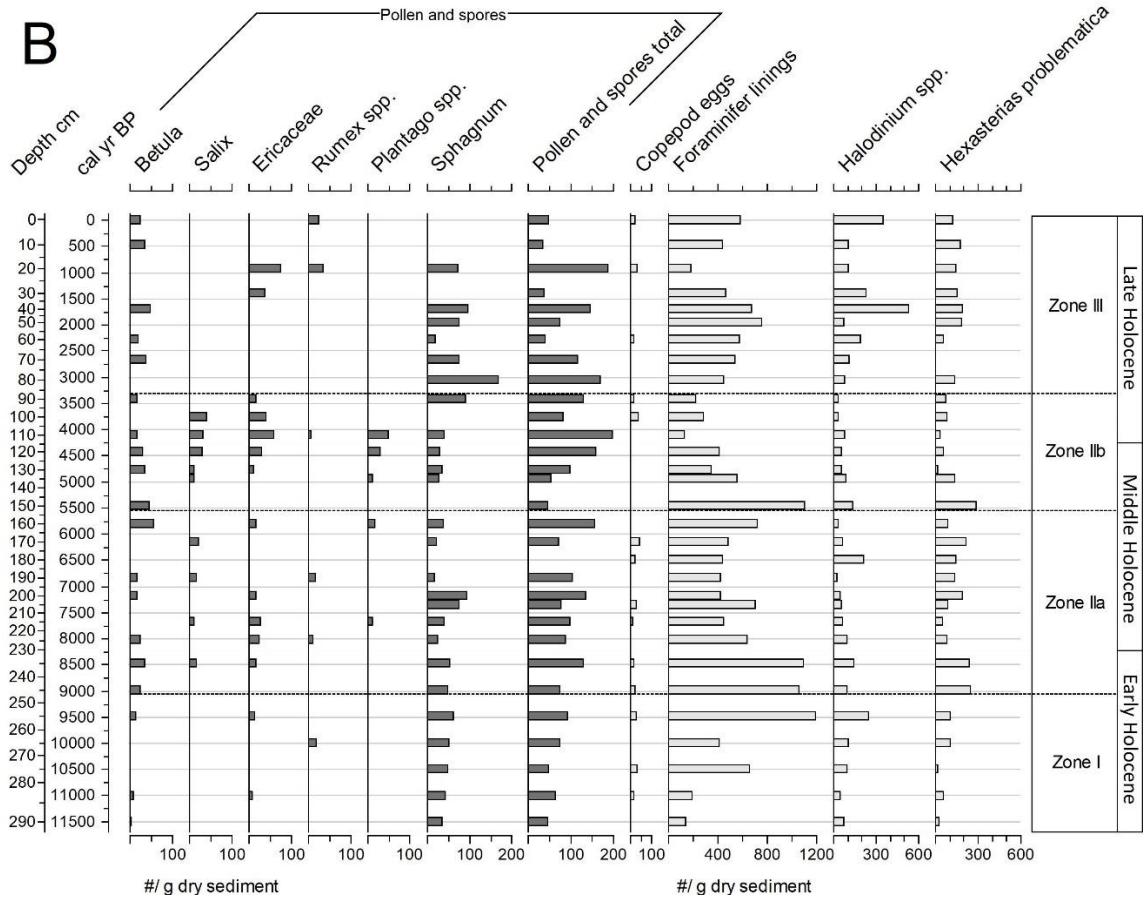

Figure 5. Relative abundances (%) of dinoflagellate cyst taxa, cyst concentration and accumulation (A), and the absolute abundances (per g^{-1} dry sediment) of main pollen, spore and other palynomorph taxa (B) in the mouth of Young Sound fjord during the Holocene, based on the Rumohr-lot core DA17-St18-213G. Zones as described in the text are divided by horizontal black dotted lines. The division between the Early, Middle and Late Holocene are determined according to Walker et al., (2019). *Operculodinium centrocarpum* includes all *O. centrocarpum* specimens: *O. centrocarpum* (process' length more than 5 µm, blue bars), *O. centrocarpum* with short processes (process' length 2-5 µm, white bars) and *O. centrocarpum* with no processes (process' length less than 2 µm, black bars). *Brigantedinium* includes *Brigantedinium simplex* (grey bars) and *Brigantedinium* spp., which could not be identified as *B. simplex* as the archeopyle was not seen (brown bars).

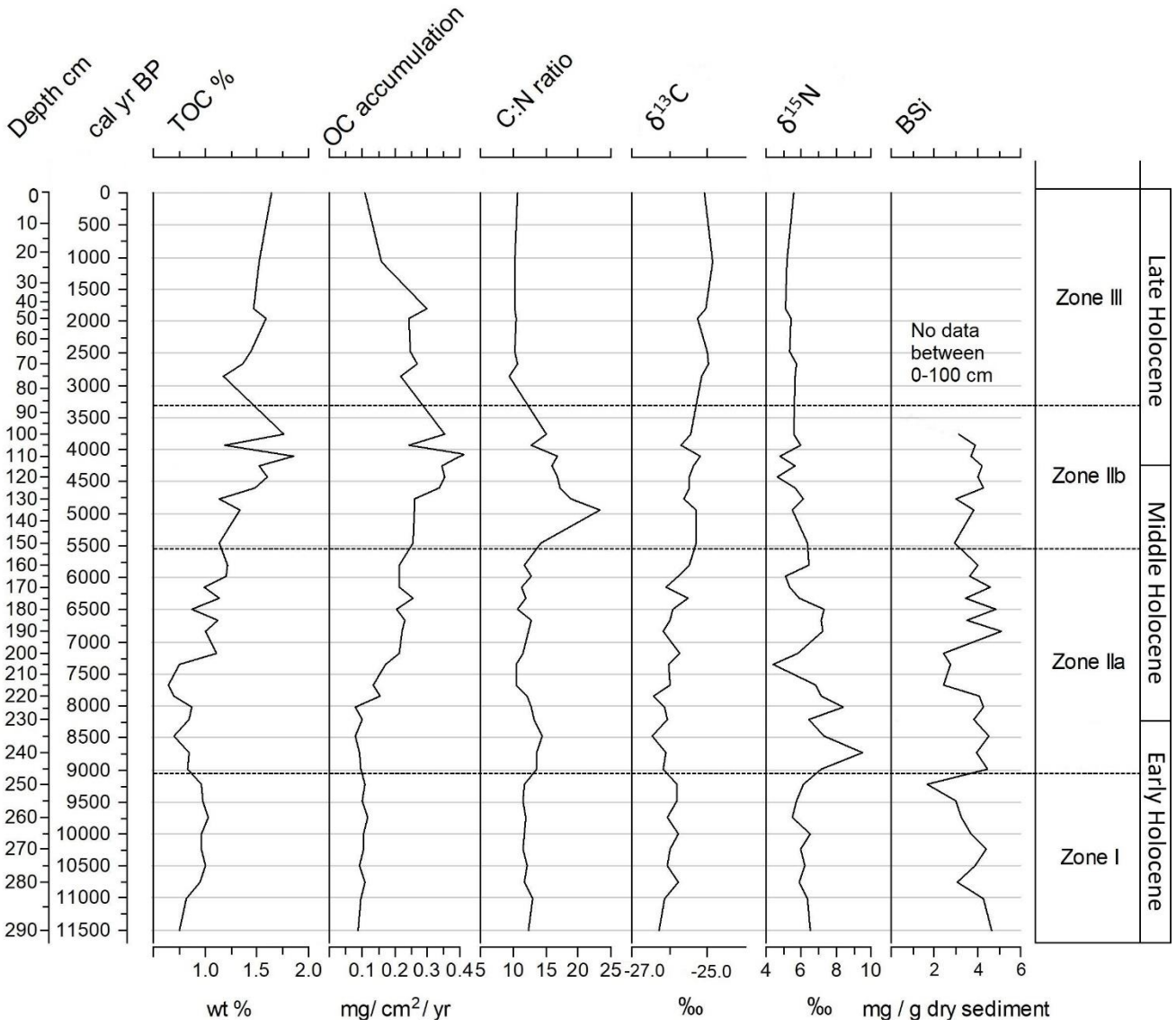

Figure 6. Geochemical results in Young Sound fjord during the Holocene, based on piston gravity core DA17-St18-213G. From left to right: TOC % (Total organic carbon, percentage-per-weight), OC accumulation (Carbon accumulation, mg/cm^2/year), C:N ratio (Carbon:Nitrogen ratio, % of carbon per % of nitrogen), $\delta^{13}C$ (carbon stable isotope, ‰), $\delta^{15}N$ (nitrogen stable isotope, ‰), and BSi (Biogenic silica concentration, mg/g^{-1} dry sample). Note that there is no biogenic silica data between 0-100 cm in the gravity core due to the lack of sediment. The Zones as described in the text are divided by horizontal black dotted lines. The division the to Early, Middle and Late Holocene for East Greenland is determined according to Walker et al., (2019).

In the topmost section above 90 cm core depth of the gravity core (Fig. 5), i.e. after 3300 years BP, phototrophic taxa – except for *O. centrocarpum* – are found only occasionally. This is the case for *Islandinium*? *cezare* as well. In this section dinocyst assemblages show more stable trends compared to the middle of the core. The relative abundances of *I. minutum* show a generally increasing trend in the top part of the core, as abundances of *E. karaense* first increase between 100 and 30 cm, and then above that, i.e. after around 1400 years BP, decrease towards the present.

The top section of the gravity core is not totally in line with the findings from the Rumohr core (Fig. 6): throughout the Rumohr core (90–20 cm core depth, i.e. approximately between 2800–470 years BP) the phototrophic taxa are more diverse. In addition to *O. centrocarpum*, particularly *Bitectatodinium tepikiense* and cf. *Diplopsalid* spp. are frequently found. *Islandinium*? *cezare*, which was found mostly between 255–100 cm core depth in the gravity core, is observed throughout the Rumohr core. The relative amounts of *I. minutum* are more stable than the ones in the gravity core, except for the notable peak at 29 cm core depth, i.e. around 800–700 years BP. At the same time period, relative abundances of *Brigantedinium* spp. and *E. karaense* decrease, and the total dinocyct concentration increases (Fig. 7). The amounts of *E. karaense* are also relatively even in the Rumohr core, except for more abundant periods at 73–53 cm core depth, i.e. roughly between 2300–1600 years BP, and at 25 cm, i.e. around 600 years BP.

Other palynomorphs identified from the samples include pollen and spores derived from high arctic vegetation (*Betula, Salix, Ericaceae, Plantago* spp. and *Rumex* spp.), tintinnid ciliates and their cysts, copepod eggs, benthic foraminiferal inner linings, and palynomorphs of unknown affinity such as *Hexasterias problematica*, *Halodinium* spp. (Figs. 5 and 7) and the occasional occurrence of *Radiosperma corbiferum*, and *Beringiella* (latter four are not included in the diagrams). *Picea* and *Pinus* pollen were also occasionally found from the sediment, but as trees never grew in East Greenland (Wagner et al., 2000), the pollen must have been transported over long distances by air or via ocean currents. Additionally, there is always a small possibility that the samples were contaminated during the laboratory preparation. The total pollen and spore abundances were relatively stable below 160 cm core depth, i.e. until approximately 5700 years BP, after which the variability increases (Fig. 5). There is a small but clear peak in the total pollen abundances around 4000 years BP (i.e. 110 cm core depth).

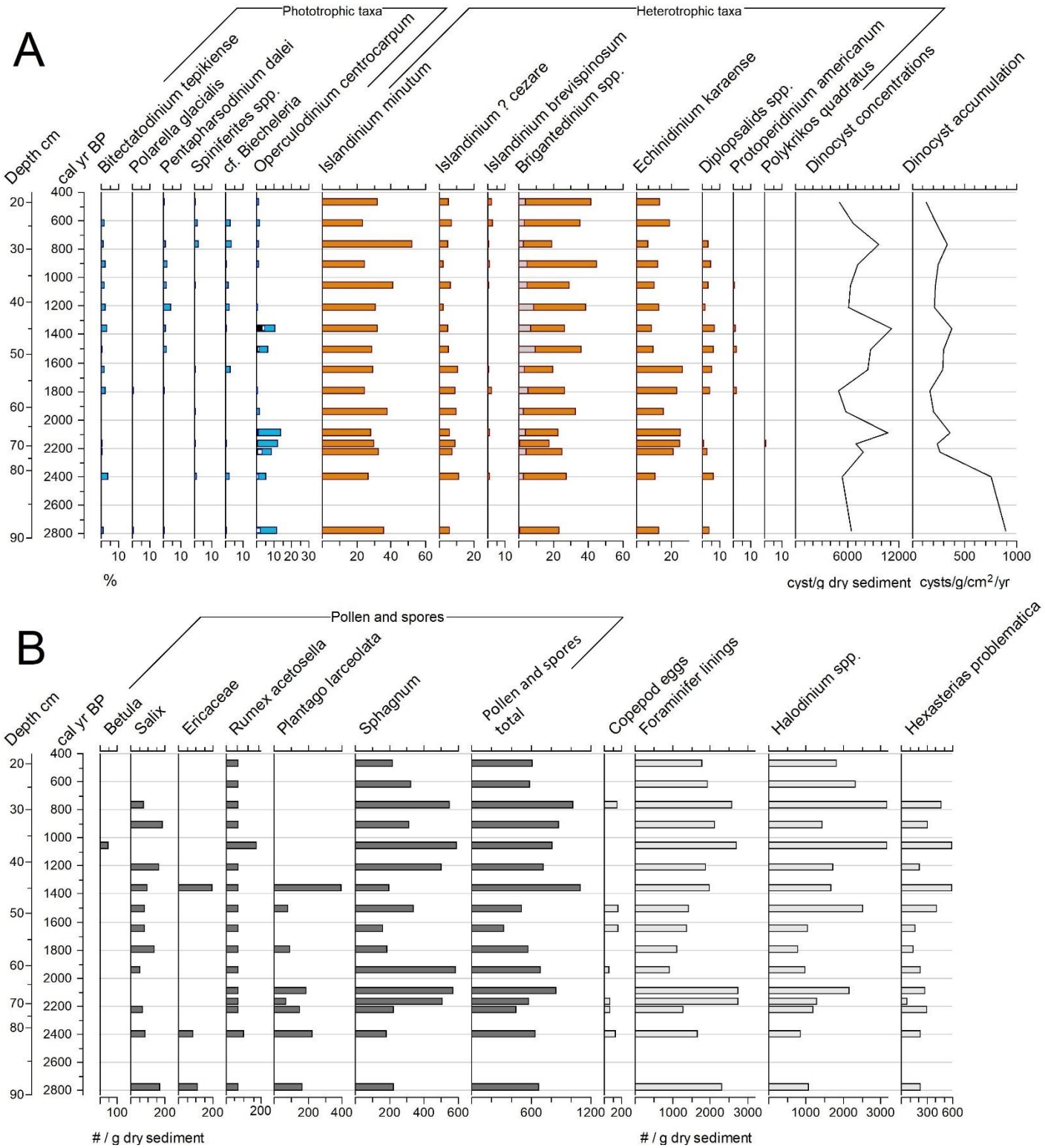

Figure 7. Relative abundances (%) of dinoflagellate cyst taxa, cyst concentration and accumulation (A), and the absolute abundances (per g^{-1} dry sediment) of main pollen, spore and other palynomorph taxa (B) in the mouth of Young Sound fjord during the late Holocene, based on the Rumohr-lot core DA17-St18-215R. *Operculodinium centrocarpum* includes all *O. centrocarpum* specimens: *O. centrocarpum* (process' length more than 5 µm, bue bars), *O. centrocarpum* with short processes (process' length 2-5 µm, white bars) and *O. centrocarpum* with no processes (process' length less than 2 µm, black bars). *Brigantedinium* includes *Brigantedinium simplex* (grey bars) and *Brigantedinium* spp., which could not be identified as *B. simplex* as the archeopyle was not seen (brown bars).

The abundances of foraminiferal linings, *Halodinium* spp. and *Hexasterias problematica* vary a lot during the Holocene, but in the gravity core there are three notable peaks when the amount of all of them increase; at 235–255 cm core depth (i.e. 9500-8500 years BP), at 150 cm (5500 years BP), and at 40 cm (1700 years BP) (Fig. 5). In the Rumohr core the abundance of total pollen and spores is relatively even, except for a clear peak around 1300–1400 years BP, i.e. 45 cm depth (Fig. 7). Foraminiferal linings and *Halodinium* spp. are at the highest levels at 65–69 cm core depth (i.e. roughly 2100-2200 years BP), at 37 cm (approximately 1100 years BP), and at 29 cm core depth (around 800 years BP).

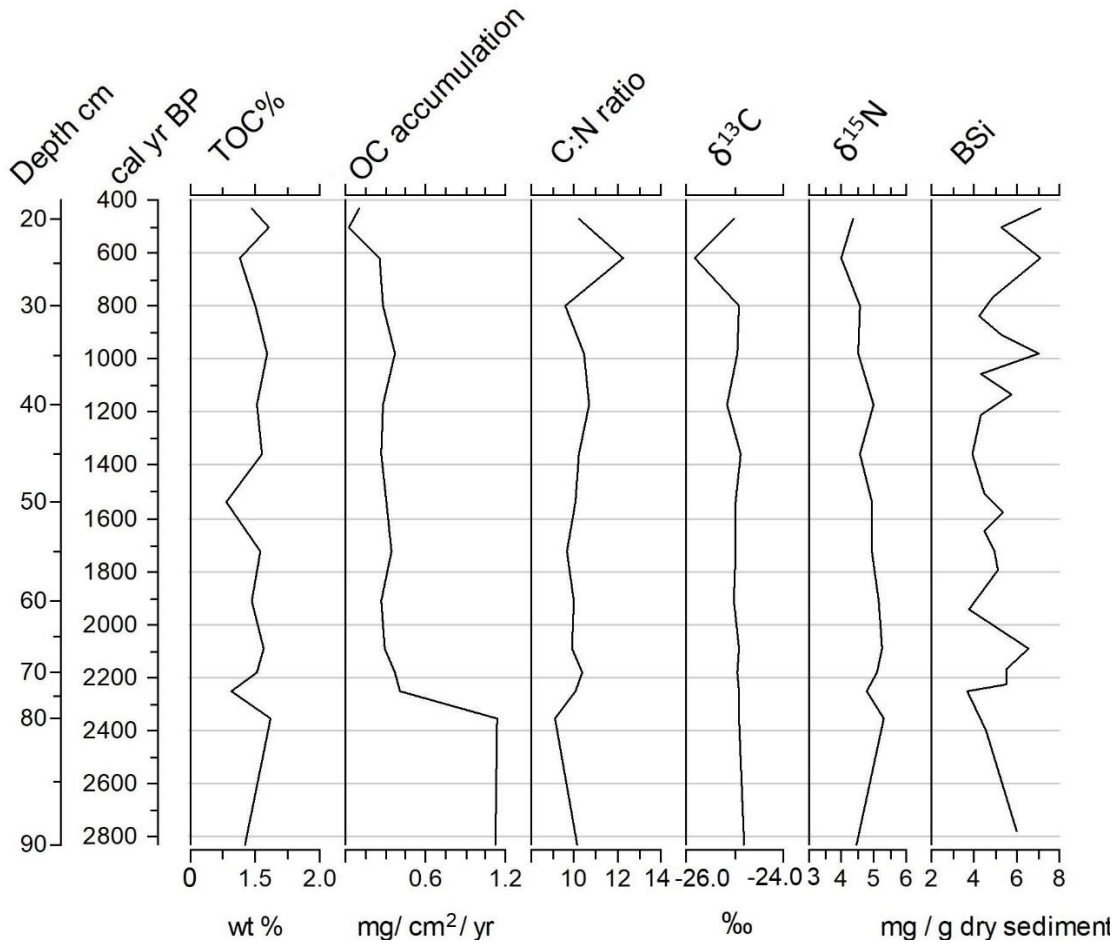

Figure 8. Geochemical results in Young Sound fjord during the late Holocene, based on Rumohr lot core DA17-St18-215R. From left to right: TOC % (Total organic carbon, percentage-per-weight), OC accumulation (Carbon accumulation, mg/cm^2/year), C:N ratio (Carbon:Nitrogen ratio, % of carbon per % of nitrogen), $\delta^{13}C$ (carbon stable isotope, ‰), $\delta^{15}N$ (nitrogen stable isotope, ‰), and BSi (Biogenic silica concentration, mg/g^{-1} dry sample).

3.3. Geochemical results

The total organic carbon (TOC) content varied between 0.70 and 1.86 wt% (percentage-by-weight, Figs. 6 and 8), and total nitrogen (TN) ranged between 0.05 and 0.16 wt%. There is a generally increasing trend in the TOC content in the gravity core throughout the Holocene. The ratio between TOC (wt%) and TN (wt%), i.e. C:N ratio, varied between 9.1 and 23.3 (Figs. 5 and 7). The $\delta^{13}C$ values ranged between -26.5 and -24.8‰ and the $\delta^{15}N$ values from 4.0 to 9.5 ‰, (Figs. 6 and 8). Total Organic Carbon%, $\delta^{13}C$, $\delta^{15}N$ and C:N variability increase between 245 and 100 cm core depth, i.e. roughly between 9000 and 3700 years BP. Highest C:N ratios are found at 135 cm core depth, i.e. around 5000 years BP (Fig. 6). Above 100 cm core depth the variability in $\delta^{13}C$, $\delta^{15}N$ and C:N decreases. Throughout the Rumohr core TOC%, $\delta^{13}C$, $\delta^{15}N$ and C:N show generally more stable values (Fig. 8).

The biogenic silica (BSi) concentrations varied between 1.7 and 7.1 mg per g^{-1} dry mass Si (milligrams of silica per one gram on dry sediment). These correspond to BSi measurements from surface sediments in Young Sound (Ribeiro et al., 2017), where BSi concentrations varied between 1.3-9.0 mg/g. Biogenic silica concentrations increase in general in the Rumohr core, whereas no clear overall trend is observed in the gravity core (Fig. 6 and 8). There are no BSi measurements from the gravity core samples above 100 cm due to the lack of sediment material.

3.4. Results from the statistical analyses

Principal component analysis (PCA) for dinocyst data, and redundancy analysis (RDA) for dinocyst and geochemical data were conducted for both cores. Figure 9 presents the biplots based on the PCA and RDA. The eigenvalues of these analyses indicate how much each axis explains of the data variation (Table 3). In the gravity core, the PCA reveals a clear negative correlation of *Brigantedinium* spp. with the first axis, meaning that the abundance of the species decreases along the axis (ter Braak, 1995, pp. 91-173). In the Rumohr core's PCA, *Operculodinium centrocarpum* correlates positively with the first axis, i.e. its abundance increases along the axis (ibid.). The second axis of the gravity core's PCA distinguishes the heterotrophic species, which correlate positively with the axis, from the phototrophic taxa, except for *I.*? *cezare*, which together with phototrophic taxa correlates negatively with the second PCA axis (Fig. 9a). However, this is not the case in the Rumohr core's PCA, which reveals that the relative abundances of *E. karaense* and *I.*? *minutum* score near each other, both negatively correlating with the second axis (Fig. 9c). Interestingly the relative

abundances of *Islandinium minutum* in the Rumohr core's data score near the origo, hence it correlates poorly (linearly) with both of the PCA axes. However, in both of the cores PCA reveals an opposite response of *I. minutum* with *O. centrocarpum* (Fog. 9a and c).

Table 3. The Eigenvalues of the first two axes in principal component analyses and redundancy analyses of the piston gravity core DA17-St18-213G (marked as light grey) and the Rumohr lot core DA17-St18-215R.

Principal component analyses			**Redundancy analyses**		
Core	Axis	Eigenvalue	Core	Axis	Eigenvalue
DA17-St18-213G	PCA 1	0.31	DA17-St18-213G	RDA 1	10.68
DA17-St18-213G	PCA 2	0.20	DA17-St18-213G	RDA 2	1.79
DA17-St18-215R	PCA 1	0.42	DA17-St18-215R	RDA 1	22.19
DA17-St18-215R	PCA 2	0.19	DA17-St18-215R	RDA 2	1.64

RDA for the gravity core reveals a positive correlation of $\delta^{13}C$ with *Brigantedinium* spp., *Echinidinium karaense* and *Islandinium minutum*. cf. *Diplopsalis* spp.,*Pentapharsodinium dalei*, *Islandinium brevispinosum*, *I.*? *cezare*, *Spiniferites* spp. and *Operculodinium centrocarpum* have a negative correlation with $\delta^{13}C$, and positive correlation with $\delta^{15}N$ and C:N ratio (Fig. 9b). TOC% seems to be in negative correlation with *E. karaense*, *I.minutum*, and *O. centrocarpum*. Also, the first two axis explain only 12.5 % of the total variation. In the gravity core's RDA BSi and OC accumulation (not presented in the biplot) score near zero indicating near zero correlation with the dinocyst assemblages. The Rumohr core's RDA also reveals a near zero correlation of OC accumulation with dinocyst species (not presented in the biplot), yet BSi correlates positively with e.g. *I.*? *cezare*, *I. minutum*, *E. karaense*, *O. centrocarpum* and *Brigantedinium* spp. (Fig. 9d). The differences of PCA and RDA results between the gravity core and the Rumohr core can be explained, at least partly, by the fact that the Rumohr core gradient is clearly shorter and the time period it covers is mainly controlled by colder conditions than the Holocene average (see chapter 1.1). The biplot graphs do not include dinocyst species that are poorly linearly related to both of the axes and/or species with a low relative abundance, as their presence in the biplot would make the figure harder to read.

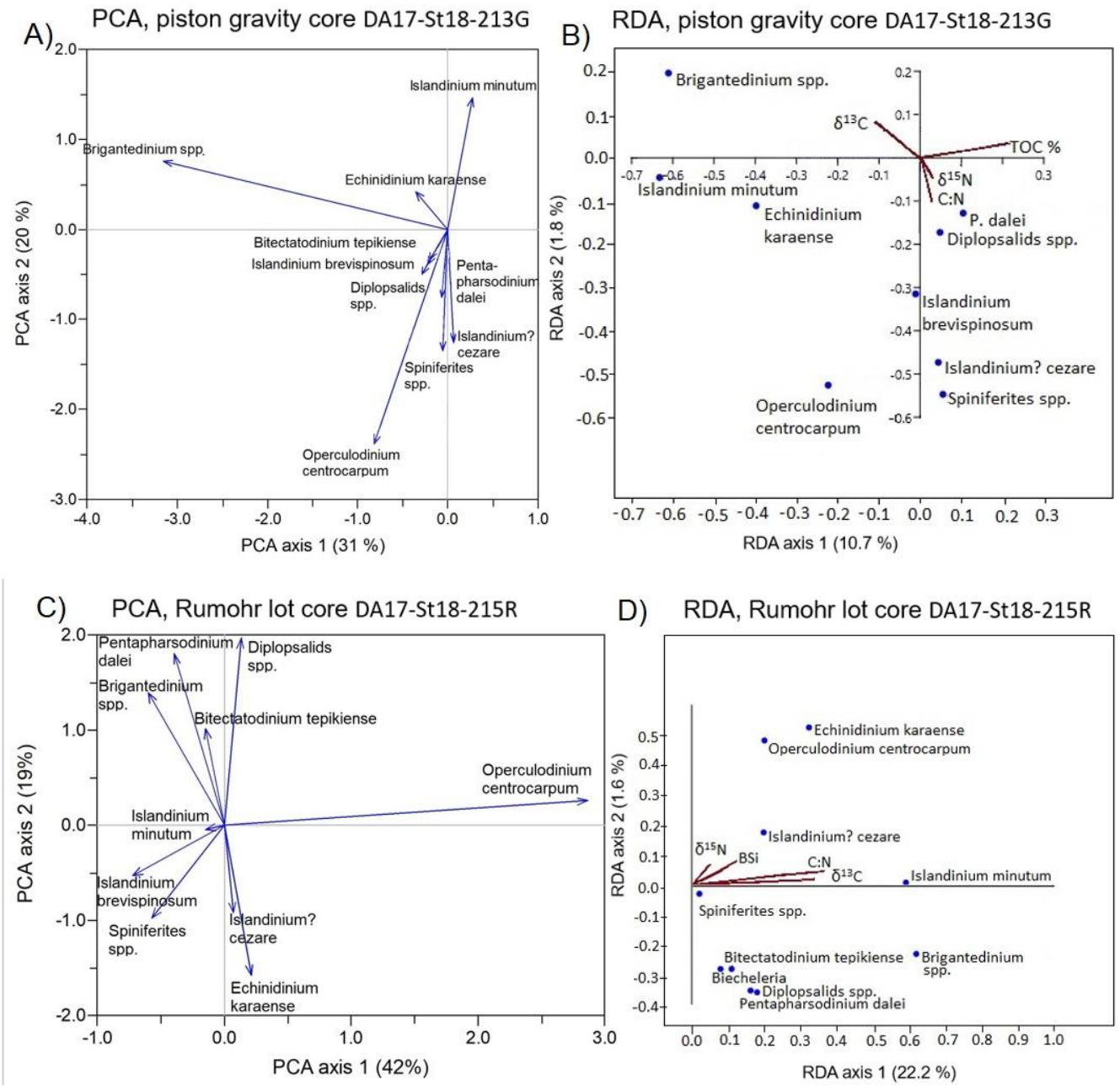

Figure 9. Biplots based on principal component analysis (PCA) of main dinoflagellate cyst taxa, and redundancy analysis (RDA) of approximate covariances of dinocyst taxa and measured geochemical variables. The above two are based on the piston gravity core DA17-St18-213G, and the two below are based on Rumohr lot core DA17-St18-215R.

4. Discussion

Four distinct zones can be recognized from the gravity core based on the major transitions in the relative amounts of the dinocyst assemblages and the geochemical variables (Fig. 5). Zone I reaches from 11500 to 9000 years BP, zone II from 9000 to 3300 years BP, and zone III from 3300 years BP to the present. Zone II is divided to sections IIa (from 9000 to 5500 years BP) and IIb (from 5500 to 3300 years BP) to further illustrate the characteristic changes in dinocyst assemblages during these intervals. The Holocene division to early, middle and late Holocene seen in figures 5 and 6 follows East Greenland climate phases of Walker et al. (2019). In the next sections, I will compare the changes in the dinocyst assemblages and other palynomorphs from the two cores from Young Sound fjord to climate and sea-ice reconstructions from Fram Strait and the Greenland Sea, and to the geochemical measurements presented in this study. As Fram Strait is a major export way of cold water masses and sea ice from the Arctic Ocean (Dahl-Jensen et al., 2011), the environmental conditions inferred there can differ a lot compared to a near-shore coastal site in the Greenland Sea. However, as marine sediment records from Northeast Greenland are very rare, studies from Fram Strait (de Vernal et al., 2013c, Werner et al., 2013, 2016, Syring et al., 2020) together with reconstructions from northeastern (Wagner et al., 2010) and southeastern (Solignac et al., 2006) Greenland give insight into the general Holocene climate and sea-ice variability in the region, to which it is interesting to compare the results presented here.

4.1. Zone I from 11500 to 9000 years BP

Highly branched isoprenoid lipids (HBIs) and phytoplankton biomarkers, foraminifera and also quantitative dinocyst reconstructions reflect reduced to variable sea-ice conditions, pro-longed open water periods and relatively high SSTs in Fram Strait between 10 500 and 9300, or up to 8500 years BP (Werner et al., 2016, Falardeau et al., 2018, Syring et al., 2020). Also, *Mytilus edulis* shells (the common blue mussel) dated to 9380-9600 years BP and found from a high Arctic lake in coastal East Greenland, illustrate warmer than present conditions in the early Holocene, as the species does not populate the area today (Wagner et al., 2010). Yet, in the study site in Young Sound, *Islandinium minutum* and *Echinidinium karaense* dominate the dinoflagellate cyst taxa in zone I, approximately between 11 500 and 9000 years BP. Both species are associated with cold SSTs and extensive sea-ice cover, and are commonly considered as sea-ice indicators (Zonneveld & Pospelova, 2015). However, even though *E. karaense* blooms during spring ice break-ups in Hudson Bay (Heikkilä

et al., 2016), recent findings do not show a clear relationship with *I. minutum* and sea-ice cover (Allan et al., 2020), and the species is found to be an open-water cyst producer in some environments (Price & Pospelova, 2011, Heikkilä et al., 2016). Phototrophic dinocyst taxa, except for *Operculodinium centrocarpum*, which is regarded as cosmopolitan (Zonneveld & Pospelova, 2015), are rare in this zone. Heterotrophic dinoflagellates can survive in dark Arctic ecosystems even with extensive sea-ice cover, as sympagic (ice associated) diatoms provide a food source for dinoflagellates blooming under ice during ice breakups in spring (Heikkilä et al., 2016). There are phototrophic, ice-associated, spring blooming dinoflagellates too (ibid.), but it is still unclear whether these taxa, cysts of *Polarella glacialis* and cf. *Biecheleria*, preserve in the downcore sediment records and have resistance to chemical sample preparation (Montresor et al., 1999, Heikkilä et al., 2016). Also the PCA and RDA distinguish phototrophic taxa and the most abundant heterotrophic taxa in the gravity core (Fig. 9).

The bottom part of the core is also characterized by very low amounts of *Brigantedinium* spp., a species complex which is often associated with high productivity, yet relatively low TOC % (ranging from 0.75–1.03 wt%) indicates low net primary production (NPP). Interestingly, BSi measurements illustrate the opposite (Fig. 6). BSi is a widely used indicator for siliceous microfossil abundance, particularly diatom productivity. Diatoms are the predominant prey for dinoflagellates, and heterotrophic dinocyst abundance in sediments is often related to their production (e.g. Pospelova et al., 2010, Heikkilä et al., 2016). The cyst production of *Brigantedinium* spp. has been observed to clearly correlate with diatom productivity (Pospelova et al., 2010, Price & Pospelova, 2011). However, the relative amounts of *Brigantedinium* in the bottom of the gravity core are low (4–15%) compared to 0–225 cm core depth, i.e. from ~8000 years BP, (9–43%, mean 26%), but the BSi values are relatively high particularly before approximately 10 000 years BP (~3.05–4.65 mg g^{-1} dry mass Si) compared to the rest of the gravity core (values ranging between 1.68 and 5.09 mg g^{-1} dry mass Si) (Figs. 5 and 6). Also, the RDA of the gravity core does not show correlation between the relative amounts of *Brigantedinium* spp. and BSi. Yet, due to methodological limitations, it is possible that some of the measured BSi is in fact detrital Si (Barão et al., 2015). As the Greenland Ice Sheet is a significant source of amorphous Si (Hawkings et al., 2017), the increased BSi concentrations could also indicate enhanced melting of the Ice Sheet during the Early Holocene. In addition to low NPP, another explanation for the low amounts of *Brigantedinium* could be that *B. simplex* cysts are produced in the late summer/fall

(Heikkilä et al., 2016). In environments with extensive sea-ice cover, the bloom can be relatively short.

The dominance of *I. minutum* and *E. karaense*, low relative amounts of phototrophic taxa as well as relatively low cyst concentrations in Zone I (Fig. 5) are often responses to harsh environmental conditions with long seasonal sea-ice cover (Zonneweld & Pospelova, 2015). However, the SST and sea-ice reconstructions from Fram Strait and East Greenland illustrate warmer than present conditions (Wagner et al., 2010, Werner et al., 2016, Falardeau et al., 2018, Syring et al., 2020). There is however recognized regionalism in Holocene sea-ice conditions in the Greenland Sea (de Vernal et al., 2013c), and it is possible that the sea surface conditions between marine versus coastal sites differ distinctly. Also, as stated in chapter 3.1, there are uncertainties related to the age-depth model and it is possible that the gravity core's ages appear approximately 700 years too young in the model. Nevertheless, the results demonstrate likely colder conditions in Young Sound during the Early Holocene than in Fram Strait or southeastern Greenland, and also low primary production. As stated before, the relatively high BSi concentrations can illustrate melting of the Greenland Ice Sheet, but as there are no signs of local freshwater input in the data, this could rather indicate regional meltwaters derived from larger-scale ice sheet retreat in the beginning of Holocene (Young & Briner, 2015).

4.2. Zone IIa from 9000 to 5500 years BP

From the late early Holocene to the mid Holocene dinoflagellate cyst taxa seem to reflect increased productivity and relatively warm SSTs with less extensive sea-ice cover. In Fram Strait, the HBI biomarkers indicate extensive sea-ice cover between 9300 and 6000 years BP (Syring et al., 2020, core PS93/02, see figure 1). However, at eastern Fram Strait (cores MSM5/5-712-2 and MSM5/5-723-2 in figure 1) the foraminifera records illustrate high productivity and relatively warm SSTs between 9000 and 5000 years BP (Werner et al., 2013, 2016), high rates of phytoplankton biomarkers and minimum IP_{25} indicate relatively warm sea surface conditions between 8500 and 7000 years BP (Müller et al., 2012), and also sea-ice reconstructions based on dinocyst records and modern analogue technique indicate minimum sea-ice concentrations during the Holocene around 7000-6000 years BP (de Vernal et al., 2013c). At the East Greenland shelf (core PS2641-4, figure 1), moderate rates of IP_{25} and high concentrations of phytoplankton markers illustrate reduced sea-ice cover between 8500 and 7000 years BP (Müller et al., 2012). Also quantitative reconstructions based

on dinocyst assemblages indicate warmer than present conditions between 9000–6000 years BP in southeastern Greenland (Solignac et al., 2006, core JM1207, figure 1).

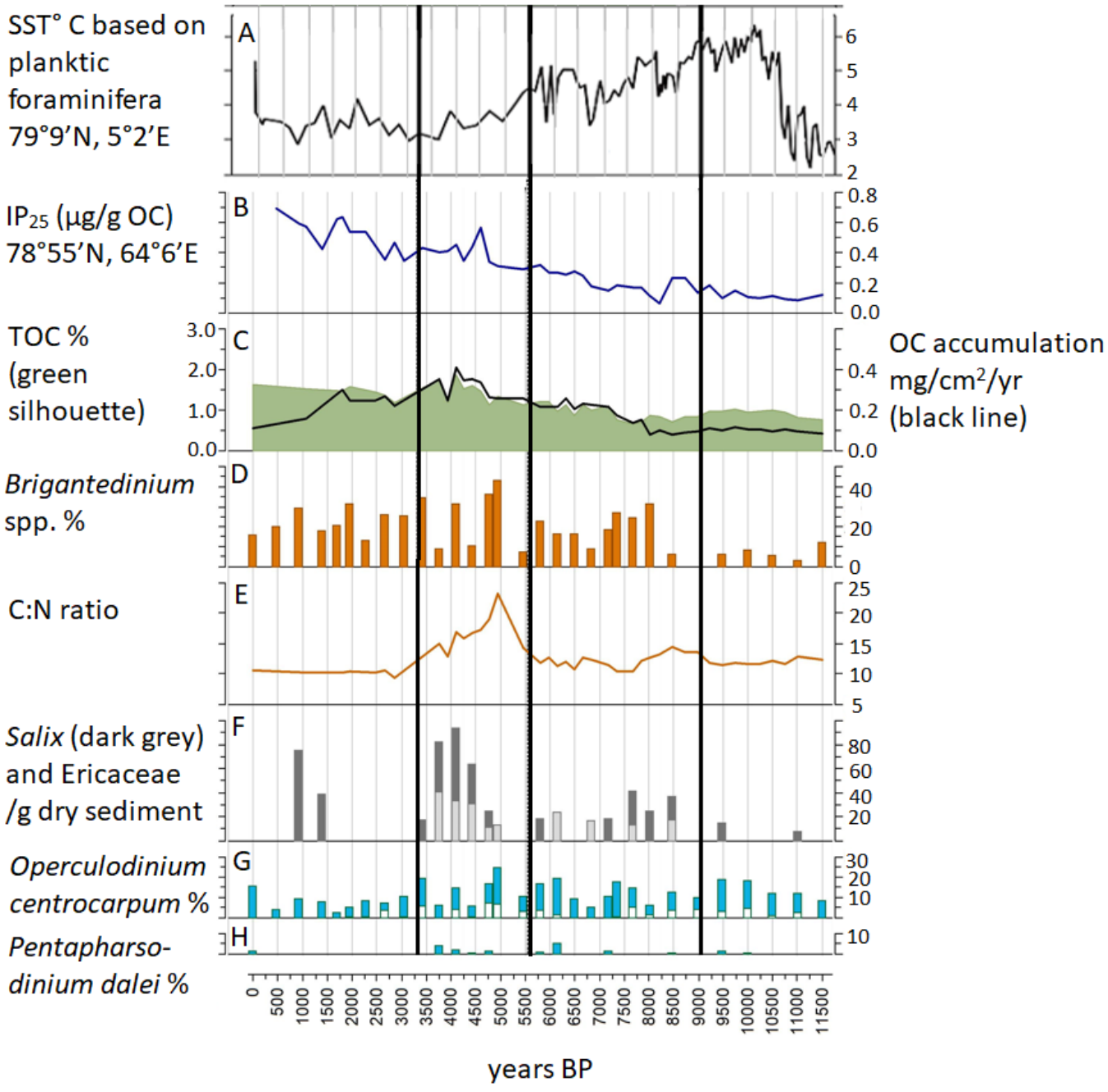

Figure 10: Summary figure showing sea surface temperature (SST) and sea-ice reconstructions from the Greenland Sea in relation to productivity indicators and the relative abundances of selected dinocyst assemblages from Young Sound fjord during the Holocene. From top to bottom: A) Summer SST °C reconstruction from Fram Strait based on planktic foraminifera (Werner et al., 2016), B) IP_{25} accumulation from Fram Strait (Müller et al., 2012), C) TOC % (Total organic carbon, percentage-per-weight, this study) and Organic Carbon accumulation (mg/cm^2/yr, this study) D) The relative amounts of Brigantedinium spp. (%, this study) E) C:N ratio (Carbon :Nitrogen ratio, % of carbon per % of nitrogen, this study), F) The abundances of *Salix* and Ericaceae, i.e. pollen from local vegetation (pollen/g dry sediment, this study), G) The relative amounts of *Operculodinium centrocarpum* (%, this study), H) The relative amounts of *Pentapharsodinium*

dalei (%, this study). The black lines distinguish the zones mentioned in the text.

In Young Sound, the geochemical results, particularly TOC, C:N, $\delta^{13}C$, and $\delta^{15}N$ show increased variability after approximately 9000 years BP (Fig. 6). This could illustrate a change from stable to relatively unstable environmental conditions, much like observed in Fram Strait between 9000 and 5000 years BP (Werner et al., 2013). The increase in species diversity in phototrophic taxa after ~9000 years BP together with more regular observations of *O. centrocarpum* with short processes and no processes, and the decrease in *E. karaense* relative abundances (between ~9000 and 7500), (Fig. 5) seem to be responses to milder conditions with shorter ice-cover period and enhanced melting in the middle Holocene. *Spiniferites elongatus*, *Spiniferites ramosus*, and *Pentapharsodinium dalei* are produced during the open water period (Heikkilä et al., 2016), and linked with increasing SSTs in the Arctic (Ledu et al., 2008) and reduced SSS's as a result of meltwaters or enhanced river discharge (Zonneveld et al., 2013). *P. dalei* is associated with environments where summer SST's are over 0 °C (ibid.), and in the Arctic it is found to negatively correlate with seasonal ice cover duration (Radi & de Vernal, 2008). This is supported by the RDA for the gravity core (Fig. 9b), where *P. dalei* correlates negatively with $\delta^{13}C$, higher amounts of which are associated with increased organic matter from ice algae sources (Søreide et al., 2006, Pineault et al., 2013, see chapter 4.4). *Bitectatodinium tepikiense* is also observed in zones IIa and IIb. The species is associated with environments where seasonal sea-ice cover is less than 4 months a year (Zonneveld & Pospelova, 2015). As stated before, shorter processes of *O. centrocarpum* have been associated with reduced salinities (Jansson et al., 2014), hence, their presence in sediments between ~ 9000–3300 years BP could also be a response to enhanced melting of the Greenland glaciers and sea ice. Also, there is a small peak in the abundances of *Halodinium* spp. and *Hexasterias problematica*, both of which are associated with enhanced terrestrial freshwater inputs (Sorrel et al., 2006, Richerol et al., 2008) (Fig. 5b).

In addition to BSi and TOC, foraminiferal linings can also be used as indirect tracers of productivity (Jorissen et al., 2007, pp. 263–325). Relatively high concentrations of BSi, and foraminiferal linings (Figs. 5 and 6) roughly between 9500 and 8000 years indicate increasing productivity, and after ~8000 years BP, there is a clear increase in the relative abundance of *Brigantedinium* spp. (Fig. 10). Also the generally increasing trend in TOC % after approximately 7500 (Fig. 10) illustrates increasing NPP. Interestingly, around 9000 and 8000 years BP there are clear peaks in both BSi and $\delta^{15}N$ ‰ (Fig. 6). Their decrease around 7500 years BP is also coupled. Lighter nitrate ($^{14}NO_3^-$) is preferred by

the phytoplankton, and hence, high relative amounts of $\delta^{15}N$ in marine sediments can reflect higher nitrate use (Limoges et al., 2020, Robinson et al., 2021). Yet, high $\delta^{15}N$ could also illustrate nitrate limitation caused by e.g. stratification, as it prevents the nutrient utilization from deeper waters (ibid.). Together with relatively high BSi, higher $\delta^{15}N$ could illustrate higher nitrate use by e.g. diatoms, yet as mentioned in the previous chapter, high BSi could also signal glacial-derived detrital Si and hence, enhanced melting of the Greenland Ice Sheet. Interestingly, this same interval is also characterised by a smaller, yet visible increase in the C:N ratio, a slight increase of local vegetation pollen (*Salix* and *Ericaceae*) and a decrease in dinocyst concentrations (Figs. 5 and 10). Together these can illustrate increased terrestrial inputs of freshwater and organic matter (see chapter 4.5). As stated in chapter 1, enhanced melting from land-terminating glaciers may increase the stratification in fjord-systems, as the freshwater from terrestrial sources creates a layer on the water surface (Murray et al., 2015, Meire et al, 2017). Thus, the increased $\delta^{15}N$ observed in the sediment between 9000 and 7500 years BP could indeed be a signal of enhanced stratification.

Interestingly, between 9000 and 6500 there is also a clear increase in the relative abundances of *Islandinium? cezare*, which is found to reflect cold SSTs in the Arctic, though the relationship between their relative amount and sea-ice cover is unclear (Zonneveld et al., 2013, Allan et al., 2020). Yet here, it seems to correlate negatively with increased $\delta^{13}C$ (Fig. 9b). The relative abundances of traditional sea-ice indicator *E. karaense* also increase between 7200 and 5500 years BP, somewhat unexpectedly, as this same time period is characterized by relatively high amounts of phototrophic taxa associated with warmer SSTs (Fig. 5). Yet *E. karaense* is also associated with low spring SSS (Zonneveld & Pospelova, 2015). Hence, the increase of species relative abundances between 7200 and 5500 years BP could also support the evidence of enhanced melting.

The dinocyst taxa and geochemical measurements from Young Sound support the findings from eastern Fram Strait and southeastern Greenland (Solignac et al., 2006, Müller et al., 2012, de Vernal et al., 2013c, Werner et al., 2013, 2016), which illustrate relatively warm sea-surface conditions and unstable or shorter sea-ice cover in the early part of the mid Holocene. The increase of C:N, local pollen and $\delta^{15}N$ also demonstrate enhanced local terrestrial melting and stratification of surface waters in zone IIa.

4.3. Zone IIb from 5500 to 3300 years BP

In zone IIb the geochemical proxies and dinocyst assemblages illustrate a continuous warm period and enhanced meltwater inputs, yet other reconstructions from Fram Strait and the southern Greenland Sea indicate a slightly cooling climate. At eastern Fram Strait, slightly increasing IP_{25} and decreasing accumulation rates of phytoplankton markers illustrate extension of the sea-ice cover and gradually reduced productivity between 7000 and 3000 years BP (Müller et al., 2012, Fig. 10). Also the foraminifera data indicate extensive sea ice after approximately 5200–5000 years BP (Werner et al., 2013, 2016), and dinoflagellate cyst taxa illustrate slightly cooling SSTs (de Vernal et al., 2013c). At the East Greenland shelf, phytoplankton markers and IP_{25} demonstrate slightly increasing sea-ice cover after approximately 6600 years BP (Müller et al., 2012). In Southeast Greenland however, the dinocyst records do not show cooling before approximately 4500 years BP, and extensive sea-ice cover after around 3500 years BP (Solignac et al., 2006).

Zone IIb between 5500 and 3300 years BP is characterized by an increased C:N ratio as well as abundances of *Salix* and Ericaceae pollen, most likely derived from local tundra vegetation (Fig. 10). These indicators together with the increased relative amounts of dinocyst taxa associated with lower SSSs (*O. centrocarpum* with shorter processes and *P. dalei*), and a small peak in the abundances of *Halodinium* spp. and *Hexasterias problematica* illustrate increasing terrestrial and freshwater inputs. During this phase, there is also a slight decrease in dinocyst concentrations and fluxes (Fig. 5). This same time period is further characterized by the most abundant relative amounts of cf. *Diplopsalis* spp. and *Spiniferites* spp. (~5000 years BP), *Brigantedinium* spp. (~5000 and ~4500 years BP), lowest relative amounts of *I. minutum* (~5000 years BP), and almost the lowest values of *E. karaense* (~5000 and 4500 years BP) during the Holocene. At 5800 and 4100 years BP cf. *Biecheleria* is also present; it is very rarely observed in the gravity core samples, and the species is associated with low SSSs. What is more, *I. brevispinosum* and Diplosalids are observed between 5000 and 4000 years BP. Interestingly, only a few observations of *I.* ? *cezare* were made from the sediment samples between ~5500–4500 years BP, but between 4500 and 4000 the species is relatively abundant when comparing with the rest of the core. From approximately 5500 to 3300 years BP also the variability in species abundances, particularly of *I. minutum*, *Brigantedinium* spp., and *O. centrocarpum* increases. As seen in figure 9b, *O. centrocarpum*, *P. dalei*, cf. *Diplopsalis* spp., *I.*? *cezare* and *Spiniferites* spp. are linked with increased C:N ratio.

Thus, much like in the zone IIa, also here increased amounts of local pollen and C:N, as well as responses of phototrophic dinocyst species associated with lower sea-surface salinity (particularly *P. dalei* and *O. centrocarpum* with shorter processes) illustrate enhanced local melting and terrestrial input of freshwater and organic matter. Yet this is not supported by most of the SST and sea-ice reconstructions from the region, which indicate colder conditions (e.g. Solignac et al., 2006, Müller et al., 2012, de Vernal et al. 2013c, Werner et al., 2013, 2016). As stated before, the environmental conditions in coastal site versus marine sites can differ distinctly, and e.g. Müller et al. (2012) noticed that the sea-ice conditions at the East Greenland shelf were less prone to variations of the oceanic circulation system than at Fram Strait. Yet, also the lake records based on e.g. macrofossils and geochemical proxies near the coast from Northeast Greenland indicate gradually cooling climate after approximately 5000–4000 years BP (e.g. Wagner et al., 2010, Wagner and Bennike, 2015). Again, it must be noted that because of the uncertainties related to the age-depth model (see chapter 3.1), timing of these events are not certain. Based on this data and the age-depth model of the Rumohr core, it seems that the gravity core sediment could be approximately 700 years too young.

4.4. Zone III from 3300 years BP to present

During the late Holocene, HBI biomarkers in Fram Strait indicate typical seasonal to marginal sea-ice conditions (Syring et al., 2020). Increased accumulation of IP_{25} illustrate extensive sea-ice cover at eastern Fram Strait after approximately 3000 years BP (Müller et al., 2012, Fig. 10). Yet, at the East Greenland shelf, IP_{25} records do not show major increase in sea-ice coverage before 1000 years BP (ibid.). As stated in the previous chapter, here, the dinocyst taxa seem to respond to cooling climate relatively late.

There is a clear change in C:N, TOC%, $\delta^{13}C$, and $\delta^{15}N$ content from highly variable to much more stable measurements particularly after ~2500 years BP, which could illustrate a change to relatively stable environmental conditions. A clear decrease in the phototrophic dinocyst taxa diversity and percentage after ~3300 years BP (Fig. 5), together with increasing relative amounts of *I. minutum* and *E. karaense* demonstrate increasing sea-ice cover. In this section, also *O. centrocarpum* with short or no processes are rare, and after ~2500 years BP, there are no observations, which could indicate a response to increased SSSs and hence depleted freshwater input from melting. The variability of heterotrophic cyst taxa, particularly *Islandinium minutum*, *Brigantedinium* spp. and

Echinidinium karense, also decreases. The relative abundances of *Brigantedinium* spp. show a decreasing trend towards the present (with a few exceptions around 2000 and 1000 years ago, Fig. 5). Together with *I. minutum* and *E. karaense*, *Brigantedinium* spp. is however one of the dominating species in the top of the gravity core. With increasing TOC % this illustrates a response to still relatively high NPP, compared to the early Holocene. Carbon isotopic composition ($\delta^{13}C$) vary relatively little during the Holocene (ranging from -27.0 to -25.2 ‰ between 11500 and 3800 years BP) but there is a clear, though small, increase after approximately 2900 years BP (values ranging from -25.5 to -24.9 ‰, Fig. 10). Generally $\delta^{13}C$ values around -27 ‰ indicate terrestrial sources of organic material, while higher values between -20 and -22 indicate aquatic sources (Meyers, 1994). However, in Arctic environments the $\delta^{13}C$ values are often lower because of slow algal growth in cold surface waters, and high pCO2 (Pineault et al., 2013). But again, as stated before, increased organic matter from ice algal sources have an opposite effect (Søreide et al., 2006). Thus, the $\delta^{13}C$ values can range from -34.7 to -18 ‰ in the Arctic (ibid.), lowest values indicating marine production and higher values indicating terrestrial or ice algae associated organic matter. As the dinocyst or pollen evidence after 2900 years BP do not indicate enhanced river discharge, i.e. freshwater input from terrestrial sources, but in fact illustrates colder conditions with depleted melting, the increase in $\delta^{13}C$ content is more likely due to enhanced ice algae production, thus also illustrating more extensive sea-ice conditions in the late Holocene. This could also be an explanation for the still relatively high TOC% and high (yet decreasing) abundances of *Brigantedinium* spp. (Fig. 10). The species correlate positively with $\delta^{13}C$ (Fig. 9b), which could be due to prey availability due to increased ice algae production.

Approximately 1000 years BP, the relative abundances of *O. centrocarpum* and *Brigantedinium* spp., both of which have had a generally decreasing trend during the late Holocene (Fig. 10) increase significantly. Simultaneously, the relative amount of *I. minutum* decreases, and together with a small peak in the amount of Ericaceae (Fig. 10), these findings could illustrate a short period of warmer SST's, possibly indicating the Medieval Climate Anomaly. This same period is not visible in the Rumohr core (Fig. 7). However, there is an increase in *O. centrocarpum* species with shorter processes around 1400 and 1500 years BP, concomitant with a clear increase in local pollen abundances and dinocyst concentrations. Together with slightly increasing TOC these could indicate an increase of terrestrial inputs. As there is an up to approximately 700 years difference in time in the gravity core compared to the Rumohr core, it is possible that these intervals in the cores do

actually overlap. A similar interval with increased local pollen amounts and relative abundances of *O. centrocarpum* with shorter processes, as well as an increase in cyst concentrations is observed around 2200–2000 years BP in the Rumohr core (Fig. 7). Generally, the Rumohr core dinocyst assemblages are consistent with the gravity core, e.g. with the same clear dominant species (*I. minutum., Brigantedinium* spp. and *E. karaense*). However, the phototrophic taxa, including e.g. *B. tepikiense* and *P. dalei*, are more diverse throughout the core. Also, the relative amounts of *I.*? *cezare* show relatively high abundances throughout the core when compared to the gravity core.

The geochemical data (i.e. increasing $\delta^{13}C$) from Young Sound demonstrate extensive and more stable sea-ice cover during the late Holocene. The decrease of the relative abundances of phototrophic dinocyst assemblages seems to be a clear response to shorter open water periods. As stated, the relatively late responses to gradual cooling based on the gravity core, could be explained by uncertainties in the age-depth models.

4.5. The influence of land-derived freshwater and organic matter inputs on productivity and dinocyst assemblages

The productivity in Young Sound, measured with TOC and BSi content, OC accumulation, and total dinocyst concentrations, was relatively low throughout the Holocene (Figs. 5–8). However, TOC % and dinocyst concentrations increase in the gravity core samples from the early to middle and late Holocene. Also, even though there are no BSi data from the top 100 cm of the gravity core, BSi content is generally higher in the Rumohr core samples from the late Holocene than in the gravity core samples from the early and middle Holocene. The dinoflagellate cyst responses support increased productivity from the middle Holocene to the late Holocene with relatively high abundances of *Brigantedinium* spp. (species associated with productivity, see e.g. Zonneveld & Pospelova, 2015). However, the carbon accumulation in the gravity and in the Rumohr core decreased after approximately 1750 and 2200 years BP, respectively (Figs. 6 and 8). Yet, as there are some uncertainties related to age-depth models, the sedimentation rates, and thus also accumulation rates may not be accurate.

The gravity core samples' bulk organic matter $\delta^{13}C$ against C:N ratio is presented in figure 11. The relatively high TOC% around 5000–2900 years BP is coupled with increased C:N ratio, which illustrates terrestrial sources of organic matter, as stated before. Here, C:N correlates positively with cf. *Diplosalis* spp., *P. dalei*, *O. centrocarpum*, *I.*? *cezare* and *Spiniferites* spp. While this is an indirect

correlation, the proxies together indicated elevated local freshwater inputs during this interval. In contrast, after 2900 years BP higher ice algal contribution to the primary production is indicated by the higher $\delta^{13}C$ values. Interestingly, even thought some of the traditional dinocyst sea-ice indicators correlate positively with $\delta^{13}C$ (*Echinidinium karaense* and *Islandinium minutum , Figs. 9b and 9d*), *Islandinium*? *cezare* has no correlation with it (Fig. 9b). This suggests that there might be different controls for the occurrence of this cold-water dinocyst species in Young Sound.

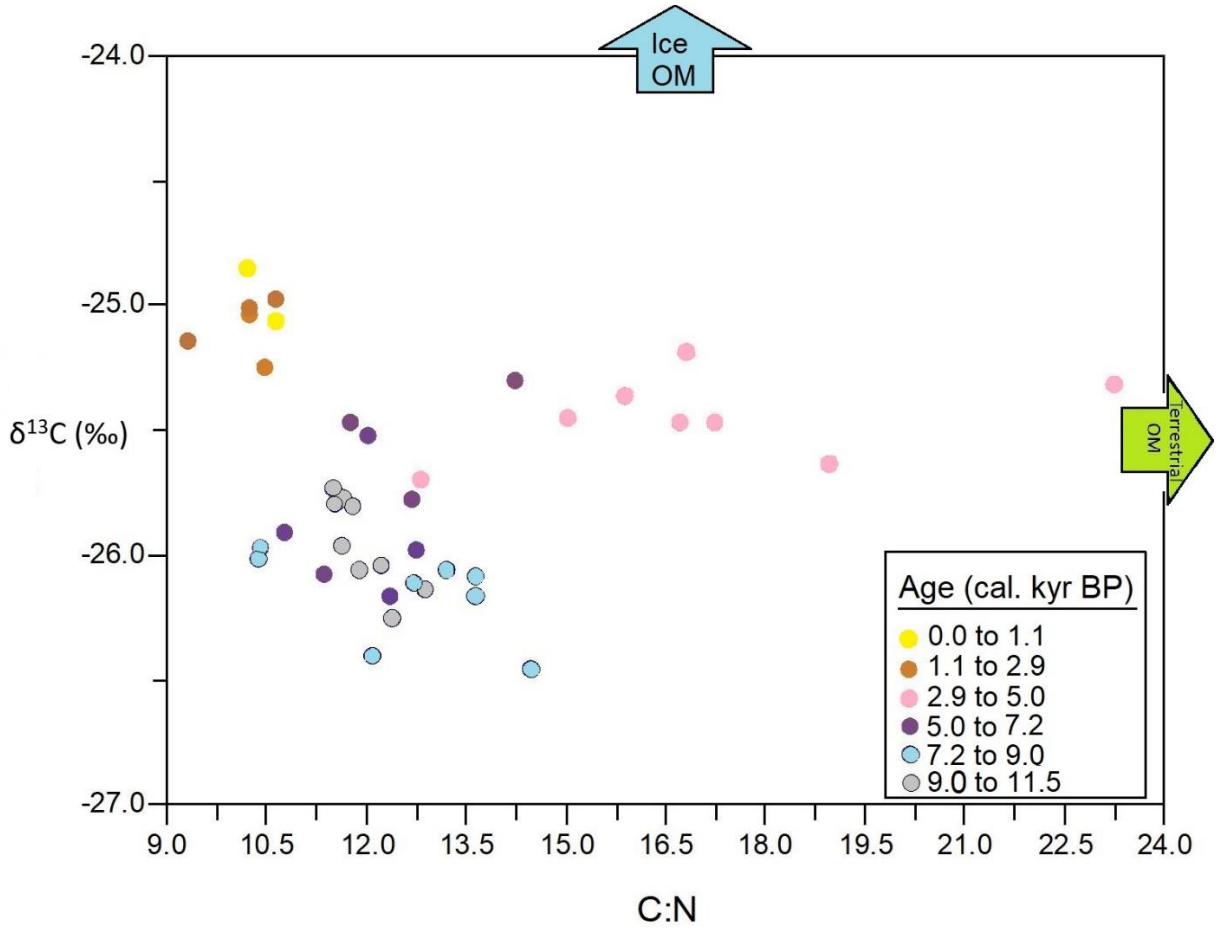

Figure 11. Organic matter carbon isotopic values ($\delta^{13}C$) against C:N ratio. The colours indicate the age of the samples in kyr (kilo years). The green arrow indicates that land-derived organic matter (OM) has usually C:N ratios over 20 (Meyers, 1994), as aquatic OM C:N ratios typically range between 4–10 (ibid.). The blue arrow illustrates that ice-derived OM that has more enriched $\delta^{13}C$ values compared to pelagic OM (Søreide et al., 2006). These data show that samples aged between 0 to 2.9 kyr contain higher values of ice-derived organic material (orange and brown circles), samples aged between 2.9 to 5.0 kyr contain higher values of land-derived OM (except for one sample aged3.9 kyr), and samples older than 7.2 kyr (blue and grey circles) contain less ice-derived and more marine OM.

It must be noted that based on the RDAs, the measured variables (i.e. TOC, OC accumulation, C:N, BSi, $\delta^{13}C$ and $\delta^{15}N$) explain only 12.5% and 23.5% of the total variation in the gravity and the Rumohr core samples, respectively (Table 3). Thus, there are environmental variables not measured here

that do control the dinocyst taxa. These likely include e.g. temperature, salinity and sea-ice concentration.

One main question of my thesis was whether the increased terrestrial freshwater input affects the ecosystem structure and productivity at the study site. As stated earlier, in fjords surrounded only by land-terminating glaciers, the terrestrial freshwater input may increase turbidity and stratification and hence, limit the light penetration and availability of deeper water nutrients (Meire et al., 2017, Kanna et al., 2018, see chapter 1). In Young Sound, this could have led to decreased proportion of phototrophic, light-dependent species, and also decreased primary productivity. However, between 9000 and 7500 and particularly between 5500 and 3300 years BP, when increased C:N, local pollen, and dinocyst species associated with decreased SSSs (Fig. 10) indicate terrestrial freshwater and organic matter input, the phototrophic taxa are relatively abundant. Yet the total dinocyst concentration and cyst accumulation rate do decrease slightly between 8500 and 7500 as well as around 5000 and 4000 years BP (Fig. 5). Also, the variability of dinocyst concentration and some dinocysts species (particularly *I. minutum*, *Brigantedinium* spp. and *O. centrocarpum*) increase clearly after 5500 years BP. These results could illustrate that the terrestrial freshwater input does affect the productivity in this particular fjord system and that the effect could be a consequence of increased stratification. This is further supported by the fact that C:N and abundances of freshwater indicator *P. dalei* seem to be linked with higher $\delta^{15}N$ (Fig 9b), which have been associated with increased stratification (see chapter 4.2). Also, small decreases in TOC% and OC accumulation rates are observed around 9000-7500, 4700 and 4000 years BP (Fig. 6), even though the general trend is increasing during these intervals. However, some of this increase can be explained by the higher amount of terrestrial organic matter in the sediments.

As mentioned above, multiple dinocyst species' relative abundance changes during the intervals of terrestrial freshwater inputs. Thus, the dinocyst species composition as a whole is clearly affected (Fig. 5). As dinoflagellates are one of the main marine primary producers (e.g. de Vernal & Marret, 2007 pp. 371–408), changes in their abundances are likely reflected in the food web. Based on this, it seems that the ecosystem structure is indeed influenced by the enhanced terrestrial inputs.

5. Conclusions

The multiproxy results in this study indicate a relatively cold early Holocene with extensive sea ice cover and low productivity, warmer and more variable conditions after approximately 9000 years BP with increasing productivity, species richness and terrestrial freshwater inputs, and colder late Holocene (after approximately 3300 years BP) with high productivity coupled with higher ice-algae contribution (Fig. 10). Thus based on this study, the ecosystem structure follows somewhat the known climate and sea ice development in the region (see e.g. 2006, Müller et al., 2012, de Vernal et al., 2013c, Werner et al., 2013, 2016, Syring et al., 2020). However, the near-shore marine ecosystem in Young Sound is clearly influenced by local forcings, such as terrestrial freshwater and organic matter inputs. This could explain the observed differences in Young Sound records compared to e.g. records form Fram Strait (Müller et al., 2012, Werner et al., 2013, 2016, Syring et al., 2020), where larger-scale forcings, such as sea-ice export from the Arctic Ocean, have greater influence.

Between 9000–7500 and 5500–3300 years BP, multiple proxies indicate enhanced terrestrial inputs of freshwater and organic matter. In fjords surrounded only by land-terminating glaciers, terrestrial inputs can increase turbidity and stratification, and thus affect the primary productivity (e.g. Meire et al., 2017). In Young Sound, TOC % and C accumulation rates show generally increasing trends during these intervals, but in contrast the total dinocyst concentration decreases indicating that the terrestrial inputs can affect at least some dimension of ecosystem productivity. During these intervals there are also clear changes in the dinocyst species composition illustrating that terrestrial inputs do affect the ecosystem structure in Young Sound. However, the increasing proportion of phototrophic dinocysts do not indicate light limitation, and hence the changes in the marine ecosystem can rather be a consequence of increased stratification.

In the future, the continuous melting of the Greenland Ice Sheet will enhance terrestrial inputs into the ocean (e.g. Meredith et al., 2019) and increase the number of fjords that are surrounded only by land-terminating glaciers. This study indicates that these developments will affect marine productivity and ecosystem structure in Greenland's fjord systems, with potential impacts on biodiversity and important fisheries. Studying past ecosystem changes in different fjord systems, and complementing marine records with proxies for terrestrial inputs, would further help constrain the future scenarios along the Greenland shore.

These results also help the paleoceanographic science community to understand how commonly used marine proxies are constrained in coastal environments. Can proxies calibrated mainly with open ocean data be used in the near-shore environments where a number of environmental variables affect the ecosystem? In this study, for example, the dinoflagellate cyst taxa commonly used as sea-ice indicators (e.g. *Echinidinium karaense* and *Islandinium*? *cezare*) were here not (solely) linked to colder climate periods, but showed responses to e.g. freshwater inputs. Also, this study underlines the indication value of dinocysts, pollen and other palynomorphs used together with basic organic geochemistry. Indeed, it seems that with these methods, together with e.g. diatoms and HBIs, it is possible to reach a comprehensive understanding when studying the coastal sites.

6. References

Andersen T.J. (2017) Some Practical Considerations Regarding the Application of 210PB and 137CS Dating to Estuarine Sediments. In: Weckström K., Saunders K. M., Gell P.A., Skilbeck C.G. (Eds.) *Applications of Paleoenvironmental Techniques in Estuarine Studies* Springer Nature, Netherlands, pp. 121–140. DOI: 10.1007/978-94-024-0990-1

Allan E., de Vernal A., Krawczyk D., Moros M., Radi T., Rochon A., Seidenkrantz M.S., Zaragosi S. (2020) Distribution of dinocyst assemblages in surface sediment samples from the West Greenland margin. *Marine Micropaleontology* 159(101818), DOI: 10.1016/j.marmicro.2019.101818

AMAP, (2017) Snow, Water, Ice and Permafrost in the Arctic (SWIPA), Arctic Monitoring and Assessment Programme (AMAP), Oslo, Norway. xiv + 269 pp.

Arrigo K.R. & van Dijken G.L. (2015) Continued increases in Arctic Ocean primary production. *Progress in Oceanography* 136(SI) pp. 60-70. DOI: 10.1016/j.pocean.2015.05.002

Bang Kvorning A. (2020) Greenland fjord productivity under climate change
- multiproxy late-Holocene records from two contrasting fjord systems (Master Thesis, University of Copenhagen).

Barão L., Vandevenne F., Clymans W., Frings P., Ragueneau O., Meire P., Conley D.J., Struyf E. (2015) Alkaline-extractable silicon from land to ocean: A challenge for biogenic silicon determination *Limnology And Oceanography-Methods* 13(7), pp. 329-344. DOI: 10.1002/lom3.10028

Bard E., Tuna T., Fagault Y., Bonvalot L., Wacker L., Fahrni S., Synal H.A. (2015) AixMICADAS, the accelerator mass spectrometer dedicated to 14C recently installed in Aixen-Provence, France. *Nuclear Instruments and Methods in Physics Research; Section B: Beam Interactions with Materials and Atoms 361*, pp. 80–86. DOI: 10.1016/j.nimb.2015.01.075

Barber D.G., Meier W.N., Gerland S., Mundy C.J., Holland M., Kern S., Li Z., Michel C., Perovich D.K., Tamura T., (2017) Arctic sea ice. In Arctic Monitoring and Assessment Programme (AMAP) *Snow, Water, Ice and Permafrost in the Arctic (SWIP*A), pp. 103-136, Oslo, Norway.

Belt S. T. (2018). Source-specific biomarkers as proxies for Arctic and Antarctic sea ice. *Organic Geochemistry* 125(1), pp. 277–298. DOI: 10.1016/j.orgge ochem.2018.10.002

Bérard-Therriault L., Poulin M., Bossé L. (1999). Guide d'identification du phytoplankton marin de l'estuaire et du golfe du Saint-Laurent incluant également certains protozoaires. Les presses scientifiques du CNRC, Ottawa, 387 p.

Bintanja R. & Selten F.M. (2014) Future increases in Arctic precipitation linked to local evaporation and sea-ice retreat. Nature 509(7501), pp. 479-492. DOI: 10.1038/nature13259

Blaauw, M., Christen, J.A., 2011. Flexible paleoclimate age-depth models using an autoregressive gamma process. *Bayesian Analogy* 6(1) pp. 457–474. DOI: 10.1214/11-BA618

Box J.E., Sharp M., (2017) Changes to Arctic land ice. In Arctic Monitoring and Assessment

Programme (AMAP), *Snow, Water, Ice and Permafrost in the Arctic (SWIPA),* pp. 137-168, Oslo, Norway.

Box J.E., Colgan W.T., (2017) Sea level rise contribution from Arctic land ice: 1850-2100. In Arctic Monitoring and Assessment Programme (AMAP), *Snow, Water, Ice and Permafrost in the Arctic (SWIPA),* pp. 219-230. Oslo, Norway.

Briner J.B., McKay N.P., Axford Y., Bennike O., Bradley R.S., de Vernal A., Fisher D., Francus P., Frechette B., Gajewski K., Jennings A., Kaufman D.S., Miller G., Rouston C., Wagner B., (2016) Holocene climate change in Arctic Canada and Greenland. *Quaternary Science Reviews* 147(SI), pp. 340-364. DOI: 10.1016/j.quascirev.2016.02.010

Brown R., Schuler V.D., Bulygina O., Derksen C., Luojus K., Mudryk L., Wang L., Yang D. (2017) Arctic terrestrial snow cover. In Arctic Monitoring and Assessment Programme (AMAP), *Snow, Water, Ice and Permafrost in the Arctic (SWIPA),* pp. 25-64. Oslo, Norway.

Dahl-Jensen D., Bamber J., Bøggild C.E., Buch E., Christensen J.H., Dethloff K., Fahnestock M., Marshall S., Rosing M., Steffen K., Thomas R., Truffer M., van den Broeke M., van der Veen C. (2011) The Greenland Ice Sheet in a Changing Climate. In AMAP (2011) *Snow, Water, Ice and Permafrost in the Arctic (SWIPA): Climate Change and the Cryosphere*. Arctic Monitoring and Assessment Programme (AMAP), Oslo, Norway. xii + 538 pp.

DeMaster D.J. (1981) The Supply and Accumulation of Silica in the Marine-Environment. *Geochimica Et Cosmochimica Acta* 45(10), pp. 1715-1732. DOI: 10.1016/0016-7037(81)90006-5

de Vernal A. and Marret F. (2007) Organic-walled dinoflagellate cysts: tracers of sea-surface conditions. In: Hillaire-Marcel, C., de Vernal, A. (Eds.), *Proxies in Late Cenozoic Paleoceanography*. Elsevier, Utrecht, pp. 371–408.

de Vernal A., Rochon A., Frechette B., Henry M., Radi T., Solignac S. (2013a) Reconstructing past sea ice cover of the Northern Hemisphere from dinocyst assemblages: status of the approach. *Quaternary Science Reviews* 79(SI), pp. 122-134 DOI: 10.1016/j.quascirev.2013.06.022

de Vernal A., Gersonde R., Goosse H., Seidenkrantz M.S., Wolff E.W. (2013b) Sea ice in the paleoclimate system: the challenge of reconstructing sea ice from proxies - an introduction. *Quaternary Science Reviews* 79(SI), pp. 1-8. DOI: 10.1016/j.quascirev.2013.08.009

de Vernal A., Hillaire-Marcel C., Rochon A., Frechette B., Henry M., Solignac S., Bonnet S. (2013c) Dinocyst-based reconstructions of sea ice cover concentration during the Holocene in the Arctic Ocean, the northern North Atlantic Ocean and its adjacent seas. *Quaternary Science Reviews* 79(SI), pp. 111-121. DOI: 10.1016/j.quascirev.2013.07.006

Ellegaard M., Lewis J., Harding I. (2002) Cyst–theca relationship, life cycle, and effects of temperature and salinity on the cyst morphology of *Gonyaulax baltica* sp. nov. (Dinophyceae) from the Baltic Sea area. *Journal of Phycology* 38(4), pp. 775–789. DOI: 10.1046/j.1529-8817.2002.01062.x

Elbrachter M., Gottschling M., Hildebrand-Habel T., Keupp H., Kohring R., Lewis J., Meier K.J.S., Montresor M., Streng M., Versteegh G.J.M., Willems H., Zonneveld K. (2008) Establishing an Agenda for Calcareous Dinoflagellate Research (Thoracosphaeraceae, Dinophyceae) including a nomenclatural synopsis of generic names. *Taxon* 57(4), pp. 1289-1303. DOI: 10.1002/tax.574019Fukuda Y., Suzaki T. (2015) Unusual Features of Dinokaryon, the Enigmatic Nucleus of Dinoflagellates. In: Ohtsuka S., Suzaki T., Horiguchi T., Suzuki N., Not F., (Eds.) *Marine Protists, Diversity and Dynamics.* Springer, Tokyo, pp. 23-45. DOI: https://doi.org/10.1007/978-4-431-55130-0

Fukuda Y., Suzaki T. (2015) Unusual Features of Dinokaryon, the Enigmatic Nucleus of Dinoflagellates. In: Ohtsuka S., Suzaki T., Horiguchi T., Suzuki N., Not F., (Eds.) *Marine Protists, Diversity and Dynamics.* Springer, Tokyo, pp. 23-45. DOI: https://doi.org/10.1007/978-4-431-55130-0

Godwin H. (1962) Half-life of radiocarbon. *Nature* 195(4845) pp. 984–984.

Hajdas I. (2008) Radiocarbon dating and its applications in quaternary studies. *Eiszeitalter und Gegenwart Quaternary Science Journal* 57(2), pp. 24

Hammer Ø., Harper D.A.T., Ryan P.D. (2001) PAST: Paleontological statistics software package for education and data analysis. *Palaeontologia Electronica* 4(1): 9pp. http://palaeo-electronica.org/2001_1/past/issue1_01.htm

Hawkings J.R., Wadham J.L., Benning L.G., Hendry K.R., Tranter M., Tedstone A., Nienow P., Raiswell R. (2017) Ice sheets as a missing source of silica to the polar oceans. *Nature Communications* 8(14198). DOI: 10.1038/ncomms14198

Head, M. J. (1996) Modern dinoflagellate cysts and their biological affinities. In: Jansonius J. & McGregor D.C (Eds.) *Palynology: Principles and Applications*, vol. 3, American Association of Stratigraphic Palynologists, Found., Dallas, pp. 1197–1248.

Heikkilä M. (2001) Siitepölyjen määritysopas. Helsingin yliopiston maantieteen laitoksen opetusmonisteita 44. Yliopistopaino, Helsinki, 34 p.

Heikkilä M., Pospelova V., Forest A., Stern G.A., Fortier L., Macdonald R.W. (2016) Dinoflagellate cyst production over an annual cycle in seasonally ice-covered Hudson Bay. *Marine Micropaleontology* 125(1), pp. 1-24 DOI: 10.1016/j.marmicro.2016.02.005

Heikkilä M., Pieńkowski A., Ribeiro S., Weckström K. (2019) Arctic Cryosphere Change and Coastal Marine Ecosystems working group. *Past Global Changes Magazine* 27(2), pp.70. DOI: 10.22498/pages.27.2.70

IPCC (2007) Climate Change 2007: Synthesis Report. Contribution of Working Groups I, II and III to the Fourth Assessment Report of the Intergovernmental Panel on Climate Change Pachauri R.K and Reisinger A.(eds.). IPCC, Geneva, Switzerland, 104 pp.

Jansson I.M., Mertens K.N., Head M.J., de Vernal A., Londeix L., Marret F., Matthiessen J., Sangiorgi F. (2014) Statistically assessing the correlation between salinity and morphology in cysts produced by the dinoflagellate Protoceratium reticulatum from surface sediments of the North Atlantic Ocean, Mediterranean-Marmara-Black Sea region, and Baltic-Kattegat-Skagerrak estuarine system. *Palaeogeography Palaeoclimatology Palaeoecology* 399(1), pp. 202-213 DOI: 10.1016/j.palaeo.2014.01.012

Jennings A.E., Knudsen K.L., Hald M., Hansen C.V., Andrews J.T. (2002) A mid-Holocene shift in Arctic sea-ice variability on the East Greenland Shelf. *The Holocene* 12(1), pp. 49–58. DOI: 10.1191/0959683602hl519rp

Jorissen F.J., Fontanier C., Thomas E., (2007) Paleoceanographical proxies based on deep-sea benthic foraminiferal assemblage characteristics. In: Hillaire-Marcel C., de Vernal A. (Eds.) *Proxies in Late Cenozoic Paleoceanography*. Elsevier, Utrecht, pp. 263-325. DOI: 10.1016/S1572-5480(07)01012-3

Juggins. S. (2007) C2 Version 1.5 User guide. Software for ecological and palaeoecological data analysis and visualisation. Newcastle University, Newcastle upon Tyne, UK. 73 pp

Kanna N. Sugiyama S., Ohashi Y., Sakakibara D., Fukamachi Y., Nomura D. (2018) Upwelling of Macronutrients and Dissolved Inorganic Carbon by a Subglacial Freshwater Driven Plume in Bowdoin Fjord, Northwestern Greenland. *Journal of Geophysical Research-Biogeosciences* 123(5), pp. 166-1682. DOI: 10.1029/2017JG004248

Kawami H., van Wezel R., Koeman R.P.T., Matsuoka K. (2009) *Protoperidinium tricingulatum* sp. nov. (Dinophyceae), a new motile form of a round, brown, and spiny dinoflagellate cyst. *Phycological Research* 57 (4) pp. 259–267. DOI: 10.1111/j.1440-1835.2009.00545.x

Kjeldsen K.K., Korsgaard N.J., Bjork A.A., Khan S.A., Box J.E., Funder S., Larsen N.K., Bamber J.L. , Colgan W., van den Broeke M., Siggaard-Andersen M.L., Nuth C., Schomacker A., Andresen C.S., Willerslev E., Kjaer K.H. (2015) Spatial and temporal distribution of mass loss from the Greenland Ice Sheet since AD 1900. *Nature* 528(7582), pp. 396–400. DOI: 10.1038/nature16183

Krawczyk D.W., Arendt K.E., Juul-Pedersen T., Sejr M.K., Blicher M.E., Jakobsen H.H. (2015) Spatial and temporal distribution of planktonic protists in the Aest Greenland fjord and offshore waters. *Marine Ecology Progress Series* 538 pp. 99-116. DOI: 10.3354/meps11439.

Kuzyk Z.Z.A., Macdonald R.W., Tremblay J.E., Stern G.A. (2010) Elemental and stable isotopic constraints on river influence and patterns of nitrogen cycling and biological productivity in Hudson Bay. *Continental Shelf Research* 30(2), pp. 163-176. DOI: 10.1016/j.csr.2009.10.014

Ledu D., Rochon A., de Vernal A., St-Onge G. (2008). Palynological evidence of Holocene climate change in the eastern Arctic: a possible shift in the Arctic oscillation at the millennial time scale. *Canadian Journal of Earth Sciences* 45(11), pp. 1363-1375. DOI:10.1139/E08-043

Lecavalier B.S., Milne G.A., Simpson M.J.R., Wake L., Huybrechts P., Tarasov L., Kjeldsen K.K., Funder S., Long A.J., Woodroffe S., Dyke A.S., Larsen N.K. (2014) A model of Greenland ice sheet deglaciation constrained by observations of relative sea level and ice extent. *Quaternary Science Reviews* 102(1), pp. 54-84. DOI: 10.1016/j.quascirev.2014.07.018Levy L.B., Kelly M.A., Lowell T.V., Hall B.L., Hempel L.A., Honsaker W.M., Lusas A.R., Howley J.A., Axford Y.L. (2014) Holocene fluctuations of Bregne ice cap, Scoresby Sund, east Greenland: a proxy for climate along the Greenland Ice Sheet margin. *Quaternary Science Reviews* 92(SI), pp. 357-368. DOI: 10.1016/j.quascirev.2013.06.024

Limoges A., Ribeiro S. Weckstrom K., Heikkilä M., Zamelczyk K., Andersen T.J, Tallberg P., Masse G., Rysgaard S., Norgaard-Pedersen N., Seidenkrantz M.S. (2018) Linking the Modern Distribution of Biogenic Proxies in High Arctic Greenland Shelf Sediments to Sea Ice, Primary Production, and Arctic-Atlantic Inflow. *Journal of Geophysical Research-Biogeosciences* 123(3), pp. 760-786, DOI: 10.1002/2017JG003840

Limoges A., Weckstrom K., Ribeiro S., Georgiadis E., Hansen K.E., Martinez P., Seidenkrantz M.S., Giraudeau J., Crosta X., Masse G. (2020) Learning from the past: Impact of the Arctic Oscillation on sea ice and marine productivity off northwest Greenland over the last 9,000 years. *Global Change Biology* 26(12), pp. 6767-6786. DOI: 10.1111/gcb.15334

Liu T., Mertens K.N., Ribeiro S., Ellegaard M.,4 Matsuoka K.,Gu H. (2015) Cyst-theca relationships and phylogenetic positions of Peridiniales (Dinophyceae) with two anterior intercalary plates, with description of *Archaeperidinium bailongense* sp. nov. and *Protoperidinium fuzhouense* sp. nov. *Phycological Research* 63 (2) pp. 134–151 DOI: 10.1111/pre.12081.

Mann E. (2002). The Value of Multiple Proxies. *Science* 297(5586) pp. 1481-1482. DOI: 10.1126/science.1074318

Marcott S.A., Shakun J.D. Clark P.U. Mix A.C. (2013) A Reconstruction of Regional and Global Temperature for the Past 11,300 Years. *Science* 339 (6124) pp. 1198-1201. DOI: 10.1126/science.1228026

Masson-Delmotte V., Schulz M., Abe-Ouchi A., Beer J., Ganopolski A., González Rouco J.F., Jansen E., Lambeck K., Luterbacher J., Naish T., Osborn T., Otto-Bliesner B., Quinn T., Ramesh R., Rojas M., Shao X., Timmermann A. (2013) Information from Paleoclimate Archives. In Stocker, T.F., D. Qin, G.-K. Plattner, M. Tignor, S.K. Allen, J. Boschung, A. Nauels, Y. Xia, V. Bex and P.M. Midgley (Eds.). *Climate Change 2013: The Physical Science Basis. Contribution of Working Group I to the Fifth Assessment Report of the Intergovernmental Panel on Climate Change*, pp. 383-464. Cambridge University Press, Cambridge, United Kingdom and New York, NY, USA.

Meire L., Mortensen J., Meire P., Juul-Pedersen T., Sejr M.K., Rysgaard S., Nygaard R., Huybrechts P., Meysman F.J.R. (2017) Marine-terminating glaciers sustain high productivity in Greenland fjords. *Global Change Biology* 23(12) pp. 5344-5357. DOI: 10.1111/gcb.13801

Meredith, M., Sommerkorn M., Cassotta S., Derksen C., Ekaykin A., Hollowed A., Kofinas G., Mackintosh A., Melbourne-Thomas J., Muelbert M.M.C., Ottersen G., Pritchard H, Schuur E.A.G., (2019) Polar Regions. In Pörtner H.-O., Roberts D.C., Masson-Delmotte V., Zhai P., Tignor M.,

Poloczanska E., Mintenbeck K., Alegría A., Nicolai M., Okem A., Petzold J., Rama B., Weyer N.M. (Eds.). *IPCC Special Report on the Ocean and Cryosphere in a Changing Climate*, pp. 203-230. In press.

Mertens K.N., Gu H.F., Gurdebeke P.R., Takano Y., Clarke D., Aydin H., Li Z., Pospelova V., Shin H.H., Li Z., Matsuoka K., Head M.J. A review of rare, poorly known, and morphologically problematic extant marine organic-walled dinoflagellate cyst taxa of the orders Gymnodiniales and Peridiniales from the Northern Hemisphere. *Marine Micropaleontology* 159(101773), DOI: 10.1016/j.marmicro.2019.101773

Mertens K.N., Verhoeven K., Verleye T., Louwye S., Amorim A., Ribeiro S., Deaf A.S., Harding I.C., De Schepper S., Gonzales C., Kodrans-Nsiah M., de Vernal A., Henry M., Radi T., Dybkjaer K., Poulsen N.E., Feist-Burkhardt S., Chitolie J., Heilmann-Clausen C., Londeix L., Turon J.L., Marret F., Matthiessen J., McCarthy F.M.G., Prasad V., Pospelova V., Hughes J.E.K., Riding J.B., Rochon A., Sangiorgi F., Welters N., Sinclair N., Thun C., Soliman A., Van Nieuwenhove N., Vink A., Young M. (2009). Determining the absolute abundance of dinoflagellate cysts in recent marine sediments: The Lycopodium marker-grain method put to the test. *Review of Palaeobotany and Palynology* 157 (3-4) pp. 238–252. DOI: 10.1016/j.revpalbo.2009.05.004

Mertens K.N., Priceb A.M., Pospelovab V. (2012) Determining the absolute abundance of dinoflagellate cysts in recent marine sediments II: Further tests of the Lycopodium marker-grain method. *Review of Palaeobotany and Palynology* 184(1), pp. 74-81. DOI: 10.1016/j.revpalbo.2012.06.012

Meyers P.A. (1994) Preservation of elemental and isotopic source identification of sedimentary organic-matter. *Chemical Geology* 144(3-4), pp. 289-302, DOI: 10.1016/0009-2541(94)90059-0 Montresor M., Procaccini G., Stoecker D.K., (1999). Polarella glacialis, gen. nov., sp. nov. (Dinophyceae): Suessiaceae are still alive! *Journal of Phycology* 35(1), pp. 186-197. DOI: 10.1046/j.1529-8817.1999.3510186.x

Müller J., Werner K., Stein R., Fahl K., Moros M., Jansen E. (2012) Holocene cooling culminates in sea ice oscillations in Fram Strait. *Quaternary Science Reviews* 47(SI), pp. 1-14. DOI: 10.1016/j.quascirev.2012.04.024

Ni Fhlaithearta S., Ernst S.R., Nierop K.G.J., de Lange G.J., Reichart G.J. (2013) Molecular and isotopic composition of foraminiferal organic linings. *Marine Micropaleontology* 102(1), pp. 69-78 DOI: 10.1016/j.marmicro.2013.06.004

Nygaard Eriksen L. (2018) Palaeoceanographic and climatic development of the NE Greenland shelf region and its impact on sediment deposition (Master Thesis, University of Copenhagen).

Overland J., Walsh J., Kattsov V., 2(017) Trends and feedbacks. In Arctic Monitoring and Assessment Programme (AMAP), *Snow, Water, Ice and Permafrost in the Arctic (SWIPA),* pp. 9-24. Oslo, Norway.

Pineault S., Tremblay J.E., Gosselin M., Thomas H., Shadwick E. (2013) The isotopic signature of particulate organic C and N in bottom ice: Key influencing factors and applications for tracing the fate of ice-algae in the Arctic Ocean. *Journal of Geophysical Research-Oceans* 118(1), pp. 287-300 DOI: 10.1029/2012JC008331

Pospelova V., Esenlulova S., Johannessen S.C., O'Brien M.C., Macdonald R.W. (2010) Organic-walled dinoflagellate cyst production, composition and flux from 1996 to 1998 in the central Starit of Georgia (BC, Canada): A sediment trap study. *Marine Micropaleontology* 75(1-4), pp. 17-37. DOI: 10.1016/j.marmicro.2010.02.003

Potvin E., Kim S.Y., Yang E.J., Head M.J., Kim H.C., Nam S. I. Yim J.H., Kang S.H. (2018) *Islandinium minutum* subsp. *barbatum* subsp. nov. (Dinoflagellata), a New Organic-Walled Dinoflagellate Cyst from the Western Arctic: Morphology, Phylogenetic Position Based on SSU rDNA and LSU rDNA , and Distribution. *Journal of Eukaryotic Microbiology* 65 (6) pp. 750-772. DOI: 10.1111/jeu.12518

Price A.M., Pospelova V. (2011) Organic-walled dinoflagellate cyst production, composition and flux from 1996 to 1998 in the central Starit of Georgia. *Marine Micropaleontology* 80(1-2), pp. 18-43.DOI: 10.1016/j.marmicro.2011.03.003

Prowse T.D., Bring A., Carmack E.C. Holland M.M., Instanes A., Mård J., Vihma T., Wrona F.J., (2017) Freshwater. In Arctic Monitoring and Assessment Programme (AMAP), Snow, Water, Ice and Permafrost in the *Arctic (SWIPA),* pp. 169-202. Oslo, Norway.

Pörtner H.O., Roberts D.C., Masson-Delmotte V., Zhai P., Tignor M., Poloczanska E., Mintenbeck K, Alegría A., Nicolai M. (Eds.) (2019). IPCC Special Report on the Ocean and Cryosphere in a Changing Climate. IPCC, Geneva, Switzerland.

Quaijtaal W., Donders T.H., Persico D., Louwye, S. (2014) Characterising the middle Miocene Mi-events in the Eastern North Atlantic realm: A first high-resolution marine palynological record from the Porcupine Basin. *Palaeogeography Palaeoclimatology Palaeoecology* 399(1), pp. 140-159. DOI: 10.1016/j.palaeo.2014.02.017

Radi T., de Vernal A. (2008) Dinocysts as proxy of primary productivity in mid-high latitudes of the Northern Hemisphere. *Marine Micropaleontology* 68(1-2), pp.84-114. DOI: 10.1016/j.marmicro.2008.01.012

Radi T., Bonnet S., Cormier M.-A., de Vernal A., Durantou L., Faubert É., Head M.J., Henry M., Pospelova V., Rochon A., Van Nieuwenhove N. (2013) Operational taxonomy and (paleo-) autecology of round, brown, spiny dinoflagellate cysts from the Quaternary of high northern latitudes. *Marine Micropaleontology* 98 pp. 41–57. DOI: 10.1016/j.marmicro.2012.11.001

Ramette A. (2007) Multivariate analyses in microbial ecology. *Fems Microbiology Ecology* 62(2), pp. 142-160. DOI: 10.1111/j.1574-6941.2007.00375.x

Reimer, P.J., Bard, E., Bayliss, A., Beck, W.J., Blackwell, P.G., Ramsey, C.B., et al., (2013). Intcal13 and Marine13 Radiocarbon Age Calibration Curves 0–50,000 Years Cal BP. *Radiocarbon* 55 (1), 1869–1887. DOI: 10.1017/S0033822200048864

Richefol T., Rochon A., Blasco S., Scott D.B., Schell T.M., Bennett R.J. (2008) Evolution of paleo sea-surface conditions over the last 600 years in the Mackenzie Trough, Beaufort Sea (Canada). *Marine Micropaleontology* 68(1-2), pp. 6-20. DOI: 10.1016/j.marmicro.2008.03.003

Robinson R.S., Kienast M., Albuquerque A.L., Altabet M., Contreras S., Holz R.D., Dubois N., Francois R., Galbraith E., Hsu T.C., Ivanochko T., Jaccard S., Kao S.J., Kiefer T., Kienast S., Lehmann M.F., Martinez P., McCarthy M., Mobius J., Pedersen T., Quan T.M., Ryabenko E., Schmittner A., Schneider R., Schneider-Mor A., Shigemitsu M., Sinclair D., Somes C., Studer A., Thunell R., Yang J.Y. (2012) A review of nitrogen isotopic alteration in marine sediments. *Paleoceanography* 27(1), pp. 1-13. DOI: 10.1029/2012PA002321

Ribeiro S., Sejr M.K., Limoges A., Heikkilä M., Andersen T.J., Tallberg P., Weckström K., Husum K., Forwick M., Dalsgaard T., Massé M., Seidenkrantz M.-S., Rysgaard S. (2017) Sea ice and primary production proxies in surface sediments from a High Arctic Greenland fjord: Spatial distribution and implications for palaeoenvironmental studies. *Ambio* 46 (1) pp. 106–118. DOI: 10.1007/s13280-016-0894-2

Ruddiman W.F. (2014) Climate archives, data, and models. In Ruddiman W.F. (2014) Earth's Climate Past and Future. W.H. Freeman and Company, New York, pp. 55-77.

Ruddiman W.F. (2014) Insolation control of ice sheets. In Ruddiman W.F. (2014) Earth's Climate Past and Future. W.H. Freeman and Company, New York, pp. 195-214.

Ruddiman W.F. (2014) Climate during and since the last glaciation. In Ruddiman W.F. (2014) Earth's Climate Past and Future. W.H. Freeman and Company, New York, pp. 273-294.

Rysgaard S., Nielsen T.G., Hansen B.W. (1999) Seasonal variation in nutrients, pelagic primary production and grazing in a high-Arctic coastal marine ecosystem, Young Sound, Northeast Greenland. *Marine Ecology Progress Series* 179(1) pp. 13-25. DOI: 10.3354/meps179013

Seidenkrantz M.-S., Andersen J.R., Andresen K.J., Bendtsen J., Brice C., Ellegaard M., Eriksen L.N., Gariboldi K., Duc C. Le, Mathiasen A.M., Nielsen T., Ofstad S., Pearce C., Rasmussen T.L., Ribeiro S., Rysgaard S., Røy H., Scholze C., Schultz M., Wangner D.J. (2017) Cruise report: NorthGreen2017 - a marine research expedition to NE Greenland onboard "R/V Dana", September 11 - October 1, 2017.

Sejr M.K., Stedmon C.A., Bendtsen J., Abermann J., Juul-Pedersen T., Mortensen J., Rysgaard S. (2017) Evidence of local and regional freshening of Northeast Greenland coastal waters. *Scientific reports* 7 (13183) pp. 1-6. DOI: 10.1038/s41598-017-10610-9

Shi G.R. (1993) Multivariate data-analysis in paleoecology and paleobiogeography – a Review. *Palaeogeography, Palaeoclimatology, Palaeoecology,* 105(3-4) pp. 199-234. DOI: 10.1016/0031-0182(93)90084-V

Solignac S., Giraudeau J., de Vernal A. (2006) Holocene sea surface conditions in the western North Atlantic: spatial and temporal heterogeneities. *Paleoceanography*
21 (2). DOI: 10.1029/2005PA001175

Søreide J. E., Hop H., Carroll M. L., Falk-Petersen S., & Hegseth N. E. (2006) Seasonal food web structures and sympagic–pelagic coupling in the European Arctic revealed by stable isotopes and a

two-source food web model. *Progress in Oceanography* 71(1), pp. 59–87. DOI: 10.1016/j.pocean.2006.06.001

Sorrel P., Popescu S.M., Head M.J., Suc J.P., Klotz S., Oberhansli H. (2006) Hydrographic development of the Aral Sea during the last 2000 years based on a quantitative analysis of dinoflagellate cysts. *Palaeogeography, Palaeoclimatology, Palaeoecology* 234(2-4), pp. 304-327. DOI: 10.1016/j.palaeo.2005.10.012

Stockmarr J. (1971) Tablets with spores used in absolute pollen analysis. *Pollen et Spores* 13 (4) pp. 615-621.

Stuiver M., Pearson G. W., Braziunas T. (1986) Radiocarbon age calibration of marine samples back to 9000cal yr bp. *Radiocarbon* 28(2B) pp. 980–1021. DOI: 10.1017/S0033822200060264

Syring N., Stein R., Fahl K., Vahlenkamp M., Zehnich M., Spielhagen R.F., Niessen F. (2020). Holocene changes in sea-ice cover and polynya formation along the eastern North Greenland shelf: New insights from biomarker records. *Quaternary Science Reviews* 231(106173), pp. 1-16.
DOI: 10.1016/j.quascirev.2020.106173

ter Braak C.J.F., Looman C.W.N (1995a) Regression. In Jongman R.H.G., ter Braak C.J.F, van Tongeren O.F.R. (Eds.) Data Analysis in Community and Landscape Ecology. Cambridgre University Press, Cambridge, pp. 29-77.

ter Braak C.J.F. (1995b) Ordination. In Jongman R.H.G., ter Braak C.J.F, van Tongeren O.F.R. (Eds.) Data Analysis in Community and Landscape Ecology. Cambridgre University Press, Cambridge, pp. 91-173.

ter Braak C.J.F., Smilauer P. (2002) CANOCO reference manual and CanoDraw for Windows user's guide: Software for Canonical Community Ordination (version 4.5). Biometris, Wageningen.

Traverse A. (2007) What Paleopalynology Is and Is Not. In: Paleopalynology. Topics in Geobiology, vol 28. Springer, Dordrecht. Pp. 1-43. DOI: 10.1007/978-1-4020-5610-9_1

Verleye T.J., Mertens K.N., Young M.D., Dale B., McMinn A., Scott L., Zonneveld K.A.F., Louwye S. (2012) Average process length variation of the marine dinoflagellate cyst Operculodinium centrocarpum in the tropical and Southern Hemisphere Oceans: Assessing its potential as a palaeosalinity proxy. *Marine Micropaleontology* 86-87(1), pp. 45-58. DOI: 10.1016/j.marmicro.2012.02.001

Wacker, L., Lippold, J., Molnár, M., Schulz, H., 2013. Towards radiocarbon dating of single foraminifera with a gas ion source. *Nuclear Instruments & Methods In Physics Research Section B-Beam Interactions With Materials And Atoms* 294(1), pp. 307-310.
DOI: 10.1016/j.nimb.2012.08.038

Wagner B., Melles M., Hahne J., Niessen F., Hubberten H.W. (2000) Holocene climate history of Geographical Society Ø, East Greenland — evidence from lake sediments. *Palaeogeography, Palaeoclimatology, Palaeoecology* 160(1-2) pp. 45–68. DOI: 10.1016/S0031-0182(00)00046-8

Wagner B., Bennike O., Bos J.A.A., Cremer H., Lotter A.F., Melles M. (2008) A multidisciplinary study of Holocene sediment records from Hjort Sø on Store Koldewey, Northeast Greenland. *Journal of Paleolimnology* 39(3) pp. 381–398. DOI: 10.1007/s10933-007-9120-3

Wagner B., Bennike O., Cremer H., Klug M. (2010) Late Quaternary history of the Kap Mackenzie area, northeast Greenland. *Boreas* 39 pp. 492–504. DOI: 10.1111/j.1502-3885.2010.00148.x

Wagner B., Bennike O. (2015) Holocene environmental change in the Skallingen area, eastern North Greenland, based on a lacustrine record. *Boreas* 44 (1), pp. 45-59. DOI: 10.1111/bor.12085

Walker M., Head M.J., Lowe J., Berkelhammer M., Bjorck S., Cheng H., Cwynar L.C., Fisher D., Gkinis V., Long A., Newnham R., Rasmussen S.O., Weiss H. (2019) Subdividing the Holocene Series/Epoch: formalization of stages/ages and subseries/subepochs, and designation of GSSPs and auxiliary stratotypes. *Journal of Quaternary Science* 34(3), pp. 173-186. DOI: 10.1002/jqs.3097

Woodgate R.A., Fahrbach E., Rohardt G. (1999) Structure and transports of the East Greenland Current at 75°N from moored current meters. *Journal of Geophysical Research* 104(C8) pp. 18059-18072. DOI: 10.1029/1999JC900146

Werner K., Spielhagen R.F., Bauch D., Hass H.C., Kandiano E. (2013) Atlantic Water advection versus sea-ice advances in the eastern Fram Strait during the last 9 ka: Multiproxy evidence for a two-phase Holocene. *Paleoceanography* 28(2), pp. 283-295. DOI: 10.1002/palo.20028

Werner K., Mullner J., Husum K., Spielhagen R.F., Kandiano E.S., Polyak L. (2016) Holocene sea subsurface and surface water masses in the Fram Strait - Comparisons of temperature and sea-ice reconstructions. *Quaternary Science Reviews* 147(SI), pp. 194-209 DOI: 10.1016/j.quascirev.2015.09.007

Young N.E. & Briner J.P. (2015) Holocene evolution of the western Greenland Ice Sheet: Assessing geophysical ice-sheet models with geological reconstructions of ice-margin change. *Quaternary Science Reviews* 114, pp. 1-17. DOI: 10.1016/j.quascirev.2015.01.018

Zonneveld K.A.F., Marret F., Versteegh G.J.M. et al. (2013). Atlas of modern dinoflagellate cyst distribution based on 2405 data points. *Review of palaeobotany and palynology* 191(SI), pp. 1-197. DOI: 10.1016/j.revpalbo.2012.08.003

Zonneveld, K.A.F. & Pospelova V. (2015) A determination key for modern dinoflagellate cysts. *Palynology* 39 (3) pp. 387- 409. DOI: 10.1080/01916122.2014.990115